DESIGN AND FABRICATION OF A MEMS CHEMICAPACITIVE SENSOR FOR THE DETECTION OF VOLATILE ORGANIC COMPOUNDS

by

Todd Jackson Plum

A thesis

submitted in partial fulfillment

of the requirements for the degree of

Master of Science in Electrical Engineering

Boise State University

June, 2006

The thesis presented by Todd Jackson Plum entitled Design and Fabrication of a MEMS Chemicapacitive Sensor for the Detection of Volatile Organic Compounds is hereby approved:

Jeff Jessing — Date
Advisor

Stephen Parke — Date
Committee Member

Wan Kuang — Date
Committee Member

John R. Pelton — Date
Dean, Graduate College

TABLE OF CONTENTS

LIST OF FIGURES

LIST OF TABLES

CHAPTER 1: INTRODUCTION

Sensors play a crucial role in protecting the public and environment from chemical threats. By detecting threats quickly and accurately, proper steps can be taken to mediate situations and minimize damage. Because of their importance, researchers have focused on the improvement of existing sensors and on the design of novel sensors. Some of the many issues that researchers and designers must consider are listed in Table 1.1.

Table 1.1. Metrics for Evaluating Chemical Sensors

- Sensitivity
- Probability of Detection
- False Positive Rate
- Response Time
- Power Consumption
- Cost
- Reliability
- Maintenance
- Durability
- Size and weight

Depending on the application, certain items in Table 1.1 are emphasized more than others. Also, there are tradeoffs between many of these issues; for example, greater sensitivity may lead to increased false positive rates (false alarms). Because of this, some researchers have focused on designing electronic “noses”. These “noses” are arrays of

different types of sensors that are networked together and may employ pattern recognition to better detect chemicals.

Focus of Thesis

The work presented in this thesis details the development of a microelectromechanical system (MEMS) sensor for the detection of volatile organic compounds, spanning from the conceptual design of the sensor through fabrication and initial testing. The unique feature of this sensor is that it detects low-permittivity analytes (relative to many other chemicapacitive polymer-based sensors, which have reported insensitivity to low-permittivity analytes). In addition, the fabrication of the sensor is relatively simple. The design was developed such that the sensor can later be monolithically integrated with CMOS sensing circuitry for improved performance. Specific goals for sensor development presented in this thesis were to:

- Design a simple, effective sensor to detect low-permittivity volatile organic compounds.
- Fabricate the sensor entirely in-house at the Idaho Microfabrication Laboratory (Boise State University cleanroom).
- Perform proof-of-concept testing to demonstrate that the sensor works as expected.

Techniques Used for Sensor Development

An exhaustive literature search on chemical microsensors was performed. This search verified that the proposed sensor design was indeed novel (no literature was found on the same design). The search gave insight into process integration and fabrication concerns, as well as device performance concerns. Lastly, potential materials were investigated, as the materials were critical in both the fabrication and functionality of the sensor. In particular, polymers were studied, as the working mechanism of the proposed sensor relied on polymer swelling.

A conceptual design of the sensor was proposed at the inception of this project by Professor Jeff Jessing. From this, a detailed design and process integration was developed. From the process integration flow, a photolithography mask set was designed and purchased.

All fabrication was done in-house at Boise State University. Fabrication tools and processes were characterized and modeled. With the individual process models, the entire sensor fabrication was modeled. Finally, sensor fabrication was performed.

Only proof-of-concept tests are presented in this thesis. These tests demonstrate that the sensor works as designed. Determining the minimum sensitivity of the sensor requires a complex testing environment, which was not available at this time. The sensors were tested by probing them on the silicon wafers that they were fabricated on (they were not packaged). A detailed description of the test set-up and results is presented in this thesis.

Structure of Thesis

This thesis is divided into seven chapters, which are briefly described below.

- Chapter 1: Introduction to project and thesis goals.
- Chapter 2: Literature review of pertinent topics to the sensor.
- Chapter 3: Details the sensor design, process integration, and materials selection.
- Chapter 4: Presents process development and modeling of equipment used to fabricate the sensors. Sensor fabrication is also modeled.
- Chapter 5: Detailed presentation of sensor fabrication.
- Chapter 6: Describes tests that were performed and results.
- Chapter 7: Provides a summary, a discussion of future work, and conclusions.

CHAPTER 2: LITERATURE REVIEW

An extensive literature search pertaining to chemical microsensors was performed. This chapter summarizes topics that are pertinent to the sensor that is the focus of this work. First, a review of polymer-based microsensors is provided. The review is limited to polymer-based microsensors because of their popularity (and in part to limit the size of the review). Relevant behaviors and properties of polymers are then discussed. Finally, due to their similarity to the developed sensor, MEMS (microelectromechanical systems) tunable capacitors are briefly discussed.

Polymer-Based Chemical Microsensors

Microsensors detect changes that are induced by target analytes (substances the sensor is designed to detect). Generally these sensors have a size limitation of being smaller than a couple of millimeters. Also, microsensors are typically built using integrated circuit (IC) and MEMS fabrication technologies. Aspects of microsensors that were important to research for this project were: sensitivity, selectivity, and ease of fabrication. These aspects directly relate to the metrics listed in Table 1.1.

While there are many different types of microsensors, a popular choice is to use polymers as the chemically active sensing component. Polymers undergo several

different physical changes when exposed to specific analytes. Sensors are designed to exploit and detect these changes. A few of the physical changes that sensors have employed are changes in (1) dielectric permittivity, (2) thickness due to swelling of the polymer, and (3) effective mass. Sensors that detect chemically induced changes, such as in dielectric permittivity or thickness, are called electrochemical sensors. Sensors that detect changes in mass are sometimes referred to as gravimetric sensors. Some electrochemical and gravimetric sensors are described below.

Electrochemical Sensors

Polymer-based electrochemical sensors use chemical interactions between polymers and analytes to induce changes in the polymer. Several different types of electrochemical sensors have been reported on. A summary of chemicapacitive, chemiresistive, and calorimetric sensors is provided in this section.

Chemicapacitive Sensors

Chemicapacitive sensors are generally composed of two conducting electrodes (of various geometrical configurations) separated by a polymer, which serves as the capacitor dielectric material. Exposure to target analytes causes changes in the polymers properties that in turn change the capacitance of the device. The magnitude of capacitive variation is often proportional to the concentration (within limits) of the target analyte that is

present. The change in capacitance alters the electrical characteristics of the device and can therefore be electrically measured.

Parallel-plate Capacitive Sensors

Two geometrical variations on capacitor electrode shape are common: (1) the parallel-plate capacitor and (2) the interdigitated electrode capacitor. Typically, with these configurations, two significant events relative to capacitive changes occur when the polymer is exposed to a target analyte. First, the polymer swells which usually acts to separate the two electrodes. This corresponds to a decrease in capacitance. Secondly, the permittivity of the polymer increases, corresponding to an increase in capacitance. A few examples of well-characterized and well-documented chemicapacitive sensors are described below.

Some of the earliest capacitive sensors were humidity sensors in which two conducting electrodes were separated by a polyamide film [1, 2]. Water, with a permittivity of approximately 76, absorbed into the polyamide, increasing the net permittivity of the polyamide. An increase in permittivity causes an increase in capacitance. For parallel-plate geometries, for the water to access the polyamide, the top electrode had to be porous. One way to do this is to use an ultra-thin metallic film, such as a 500Å coating of gold reported in [3], for the top electrode. An electrode of this nature is effectively transparent to moisture. Another way to create a porous electrode is to simply etch slits or holes in the top electrode, as reported in [2]. Humidity sensors

were eventually fabricated with CMOS circuitry to improve sensitivities to approximately 1% relative humidity [4, 5].

Chemicapacitive sensors to measure the swelling of films have been reported in [6, 7], which act as pressure sensors. These sensors are parallel-plate capacitors, formed between the substrate (bottom electrode) and a silicon membrane (top electrode), which is separated by an air gap. Figure 2.1 shows a cross-section of this type of sensor (pressure is applied by the swelling polymer).

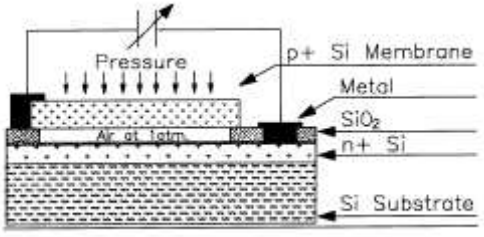

Figure 2.1. Parallel-plate pressure/chemical sensor [7]

To make the structure in this figure a sensor, the silicon membrane is coated with a chemically sensitive polymer, which is then coated with a rigid, porous material. When an analyte is present, it travels through the porous material and absorbs into the polymer, causing it to swell. The swelling pushes the membrane towards the bottom electrode, causing the capacitance to increase. While this device was initially developed to measure the pressure of the swelling film, it was later employed as a chemical sensor, as the swelling was proportional to the analyte concentration.

A different type of parallel-plate capacitor has been developed to detect changes in dielectric permittivity [8-10]. For this sensor, as opposed to the previous one (Fig. 2.1), the chemically sensitive polymer serves as the capacitor dielectric separating the to electrodes, as shown in Fig. 2.2.

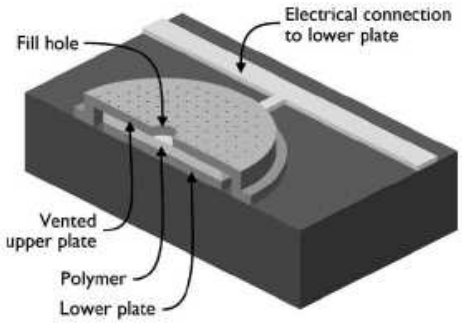

Figure 2.2. Parallel-plate capacitive sensor for dielectric permittivity changes [8]

In effort to maximize detection of dielectric permittivity changes, a system of anchoring the top electrode to the substrate was used, which acted to prevent the swelling polymer from pushing the electrodes apart. This sensor was fabricated as air-gap parallel-plate capacitor. A large hole was etched in the center of the top electrode so that the capacitor can be filled (post-fabrication) with a diluted polymer via injection. The smaller holes in the top electrode (seen in Fig. 2.2) are necessary to remove a sacrificial oxide that is used in making the air-gap capacitor. All of the holes in the top electrode provide access for the target analyte to the polymer. The sensor was integrated monolithically with CMOS sensing circuitry. Some reported performance specifications for this sensor are a lower detection limit of 100ppb when detecting DMMP with a SXFA

polymer and a response time of 15.8 seconds. This sensor has been tested with many different polymers and simulants and is now commercially available from SEACOAST Sciences [10].

Interdigitated Capacitive Sensors

A novel implementation of interdigitated electrodes allows for a permittivity change or swelling to be detected based on the thickness of polymer [11-17]. Figure 2.3 shows a diagram of this interdigitated sensor prior to polymer deposition with the two electrodes labeled as E1 and E2. The polymer was applied the to electrodes by spraying it through a mask. Figure 2.3 shows a diagram of this sensor with thin and thick polymer coatings.

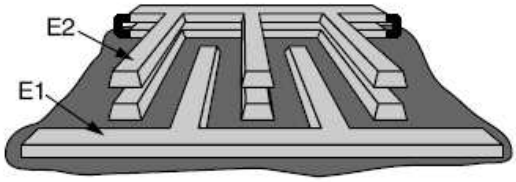

Figure 2.3. Interdigitated capacitive sensor prior to polymer application [11]

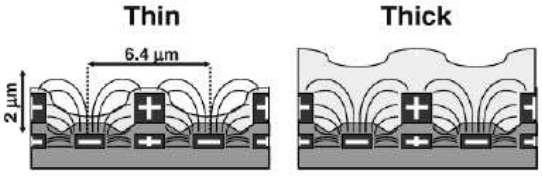

Figure 2.4. Interdigitated capacitor with polymer coatings [12]

As shown in Fig. 2.4, when a thin polymer coating is used, the electric field lines pass through some air and some polymer. When the polymer is exposed to an analyte, it swells and displaces some the region that was air (where the electric field lines pass

through). Depending on the permittivity of the analyte relative to the polymer, the capacitance can increase or decrease (based on swelling). When the sensor is covered with a thick polymer coating, almost all of the electric field lines pass through the polymer. Swelling is negligible in this configuration and the change in permittivity will dominate. This sensor was integrated on the back end of a CMOS delta-sigma sensing circuit.

Chemiresistive Sensors

Chemiresistive sensors measure the electrical resistance through a polymer between two electrodes. Typically the polymer is an insulator that is mixed with conductive black carbon. When the polymer swells, the arrangement of the black carbon molecules changes, which changes the effective resistance of the polymer [18-22]. While these are relatively simple devices, the uncertainty of where the analyte absorbs into the polymer (near the contacts or in the bulk of the polymer) makes determining a precise analyte concentration difficult [22]. Sensitivity of these sensors has been increased by integrating them on-chip with CMOS circuitry [21]. In addition, it is common to use arrays of these sensors in effort to increase selectivity [21].

Thermal (Calorimetric) Sensors

Calorimetric sensors have been reported on that senses changes in enthalpy during absorption or desorption of an analyte into or from a polymer [11, 23, 24]. This is done by using thermocouples to measure the difference between a polymer-coated n-well island and the substrate, which makes use of the Seebeck effect [11]. Not many calorimetric sensors have been reported on.

Mass (Gravimetric) Sensors

Polymer-based gravimetric sensors use a change in polymer mass to alter an electrical signal.

Surface Acoustic Wave (SAW) Sensors

Surface acoustic wave (SAW) sensors are composed of input transducers, output transducers, and chemically sensitive polymers on a piezoelectric substrate, as shown in Fig. 2.5 [25-27].

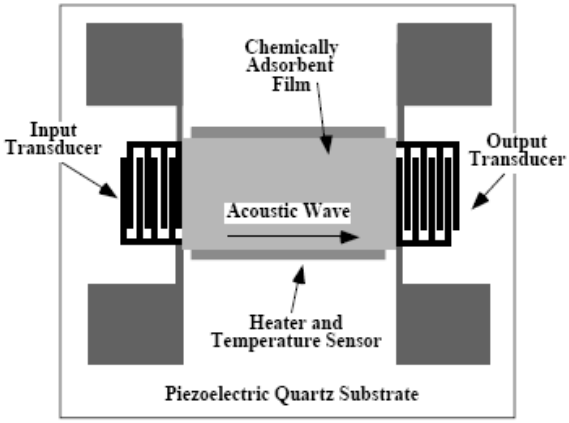

Figure 2.5. SAW chemical sensor [18]

Due to the nature of piezoelectric materials, an electrical signal (at the input transducer) generates a mechanical wave in or on the substrate. The wave propagates through the substrate to the output transducer, where the mechanical wave is converted back into an electrical signal. A SAW device is converted into a sensor by coating the substrate with a chemically sensitive polymer. When the polymer absorbs an analyte, its mass increases. This additional mass on the substrate will decrease the velocity of mechanical waves propagating through the substrate, which corresponds to a phase change in the electric signal generated at the output transducer. Sensitivities of parts-per-trillion (ppt) have been demonstrated with SAW sensors [28]. A very common piezoelectric substrate is quartz, however, piezoelectric films, such as aluminum nitride and zinc oxide, can be deposited on silicon substrates so the CMOS sensing circuitry can be monolithically integrated with SAW sensors [29].

Cantilever (Resonant Beam) Sensors

A cantilever sensor is a small, suspended, polymer-coated beam that oscillates at a resonant frequency [11,30-33]. When analytes absorb into the polymer, its mass increases and this causes a change in the resonant frequency, which can be electrically sensed. Cantilever sensors have reported detection of analyte concentrations of volatile organic compounds of less than 1ppm [11]. Also, power consumption in the nanowatt range has been reported [30].

Polymer Use for Chemical Sensors

Because the sensor in thesis is a polymer-based sensor, a basic review of polymer terminology is provided. These items that are discussed are related to how well an analyte will absorb into and diffuse through a polymer. Following the terminology review is a discussion of polymer/analyte interactions as well as topics important to choosing polymers for chemical sensors.

Polymer Chemistry

A polymer is composed of a chain of repeated unit molecules called “mers” (polymer = many mers). A mer is analogous to a unit cells in crystallography – that is, it is the smallest repeatable unit in a system. A copolymer is composed of two or more different

mer structures. The molecular structure of polymers can be divided into four general categories [34]:

1. Linear Polymers: linear polymers contain mer units that are bonded back-to-back to form long chains, sometimes described as strings of spaghetti.
2. Branched Polymers: branched polymers have chains extending off of a central chain, similar to how tree branches protrude from the tree trunk.
3. Cross-linked Polymers: cross-linked polymers contain linear or branched polymer chains that are covalently bonded to adjacent polymer chains.
4. Network Polymers: network polymers exist when a single mer molecule has several covalent bonds attached to it (versus one or two covalent bonds for structures (1)-(3)).

Often times, a polymer can contain several different types of molecular structures simultaneously. The molecular structure of a polymer directly affects how well molecules diffuse through a polymer and how much a polymer will swell.

Polymers can be defined by their many physical properties. It is helpful to review some of these definitions when considering a polymer for use in a chemical sensor. Below is a list of some useful terminology:

- Crystallinity: polymer crystallinity refers to the organization of a polymer's molecular chains. The degree of crystallinity depends on the molecular structure of the polymer and on some synthesis/processing procedures, such as allowing the ample time for the polymer to cool after it has been heated.

- Diffusivity: the diffusivity of a polymer describes how well a foreign substance can travel through the polymer. The degree of diffusivity is largely determined by the permeability of the polymer and its adsorption characteristics. Molecular structure plays a key role as well. For example, amorphous polymers have larger diffusivities than crystalline polymers.
- Melting Temperature: the melting temperature of a polymer occurs when the polymer changes from a solid to a liquid state upon heating.
- Glass Transition Temperature: the glass transition temperature describes the transition from a rigid solid to a rubbery state when heating. The glass transition occurs in amorphous and semi-crystalline polymers.

Polymer/Analyte Interaction

The adsorption of an analyte into a polymer can be described in three steps [35]:

1. A cavity forms/exists in the polymer
2. An analyte diffusing through the polymer fills the cavity
3. Attractive interactions between the polymer and analyte form. The attractive interactions that can form between the polymer and analyte are [35]:
    - Induced dipole/induced dipole interactions (also called London dispersion interactions)
    - Dipole/induced dipole interactions (also called dipole induction interactions)

- Dipole/dipole interactions (also called dipole orientation interactions)
- Hydrogen bonding interactions

It is desirable for chemical sensors that interactions between the analyte and polymer be reversible.

The absorption of an analyte into a polymer will induce physical changes in the polymer. Some of the significant changes pertaining to sensor design are:

- Change in volume (swelling). The absorption of an analyte causes a net repulsion of the polymer chains [36].
- Change in dielectric permittivity.
- Change in mass.
- Change in index of refraction.
- Calorimetric change.

Many different sensors, some which have been described, have been designed to detect the change in one or more of these physical properties.

Polymer Selection for Chemical Sensors

The basis of using polymers in chemical sensors is that the polymer must be able to absorb a target analyte. However, for a given polymer, generally only a certain type of analyte can be absorbed by that polymer; that is, some sort of compatibility must exist between the polymer and analyte. Methods to predict and quantify this compatibility have been developed. Sometimes the use of a single parameter is sufficient. Examples

of single parameter methods are the Partition Coefficient or the Hansen Solubility Parameter. However, a more precise method to predict compatibility of a polymer and analyte is to use the linear solvation energy relationship (LSER) equation. These methods are described below.

Hildebrand and Hansen Solubility Parameters

Hildebrand and Hansen solubility parameters provide some insight into how soluble a material is into another material. Hildebrand defined a single solubility parameter in 1936, and Hansen later subdivided this parameter into a polar, dispersion, and hydrogen bonding component. The general idea is that for an analyte and polymer with similar Hansen solubility parameters, the analyte is likely to absorb into the polymer [37]. A concern with this method is that sometimes materials with dissimilarities have similar solubility parameters [35].

Partition Coefficient

The partition coefficient is a thermodynamic parameter that measures the concentration of analyte in the gas phase near the surface of the polymer to the concentration of analyte in the polymer (at equilibrium) and is defined as:

$$K = \frac{C_p}{C_v}$$

where K is the partition coefficient, C_p is the concentration of the analyte in the polymer and C_v is the concentration of the analyte in the gas phase above the polymer surface.

The partition coefficient can be derived from the standard Gibb's free energy [35]. As with the Hildebrand solubility parameter, because the partition coefficient is only a single term (which can fail to account for some physical phenomena) it can lead to inaccurate conclusions.

Linear Solvation Energy Relationships (LSER)

The linear solvation energy relationship (LSER) equation describes and quantifies various interactions between the polymer and analyte [35, 28]. This equation has been applied in detail to SAW chemical sensors [25]. The LSER equation is defined as [35, 38]:

$$\log K = c + r_P R_A + s_P \pi_A + a_P \alpha_A + I_P \log L_A$$

The subscripts *P* and *A* specify whether parameter applies to the polymer or analyte. A brief description of the parameters is provided below:

Table 2.1. Descriptions of LSER Coefficients

Parameter	Description
K	Partition Coefficient
c	A constant resulting from multiple linear regression analysis of logK values
r_P	Measures polymer polarizability
R_A	Models polarizablitity of analyte
s_P	Measures polymer dipolarity/polarizability

π_A	Measures analyte dipolarity/polarizability
a_P	Measures polymer hydrogen-bond basicity
α_A	Measures analyte hydrogen-bond acidity
I_P	Describes the energy relating to forming a cavity in the polymer for the analyte as well as the dissolution of the analyte from the polymer
$logL_A$	Describes the energy relating to forming a cavity in the polymer for the analyte as well as the dissolution of the analyte from the polymer

The listed references show that the LSER method is remarkably accurate. The difficulty of this method can be determining the parameters in Table 2.1. The references list values for many different polymers and analytes related to chemical sensors; however, employing this method for research groups wanting to experiment with materials not listed in the references could be challenging as they would have to determine all of the parameters.

MEMS Tunable Capacitors

The sensor described in this thesis requires a parallel-plate capacitor to be modified such that the top electrode is free to move towards and away from the bottom electrode. Another device that does this is a MEMS tunable capacitor. A tunable capacitor is desirable for various applications such as phase-locked-loop (PLL) circuits

[39]. A common method of making a tunable parallel-plate capacitor is to suspend the top electrode with spring structures so that it can move [39-42]. This is shown in Fig. 2.6.

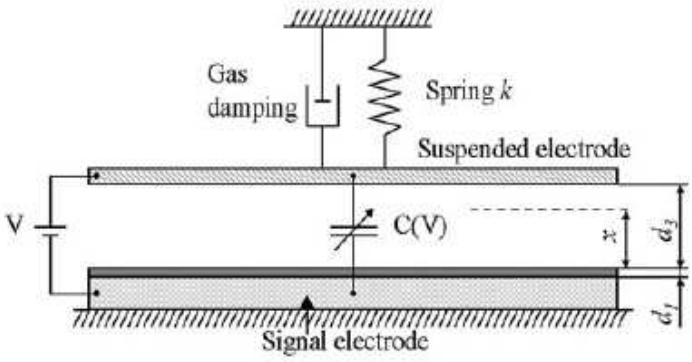

Figure 2.6. MEMS tunable capacitor with flexible electrode [40]

Typically the most desirable dielectric medium for a tunable capacitor is air. This is because air provides the least mechanical resistance for moving the electrode through. The gap between the electrodes is modulated by applying a DC voltage across the electrodes [42]. The idea of a flexible top electrode will be used in the sensor detailed in this thesis.

Summary

The literature review performed for this thesis work showed that polymer-based microsensors offer high-sensitivity, low-power operation, and are potentially inexpensive (if bulk manufactured as many IC's are), especially if the sensors are integrated monolithically with CMOS sensing circuitry.

Concepts relating to polymer-analyte interactions were reviewed such that an appropriate polymer can be selected to detect the desired substance.

A review of MEMS capacitive devices gave insight to the idea of using movable capacitor electrodes to modulate the electrical characteristics of the capacitor. The suspension of the top electrode in a parallel plate capacitor configuration as done with most tunable capacitors will be employed in the sensor detailed in this thesis.

A prevalent concept that emerged throughout the review is that none of the chemical sensors were 100% selective. However, different types of sensors are capable of measuring different changes in the polymer properties. Ultimately, arrays of different types of sensors (electronic noses) are desirable in effort to improve performance in all aspects.

CHAPTER 3: SENSOR DESIGN, MATERIALS, & PROCESS INTEGRATION

This chapter discusses the design of the sensor and its theoretical operation. The fabrication steps required to build the sensor are presented, including a discussion on material selection for the sensor.

Sensor Design

Design Objectives

The main objectives of the sensor design are that:

- The sensor measures the swelling of a polymer film.
    - The sensor detects volatile organic compounds in the gaseous (vapor) phase. These compounds are referred to as target analytes for the remainder of this thesis.
    - Specific analytes can be targeted by choosing appropriate polymers.
- The sensor fabrication is as simple as possible.
    - A simple design often corresponds to a low cost design, due to a reduction in processing steps and time.

- The sensor fabrication is compatible with CMOS fabrication technology
    - This enables the potential integration of CMOS sensing circuitry with the sensor for improved sensing performance.

These objectives were the foundation from which design decisions were made throughout the development of the sensor, which is described in the remainder of this chapter.

Physical Structure and Theoretical Operation

The sensor is a parallel-plate capacitor composed of two planar and parallel electrodes separated by a thin polymer dielectric film. Neglecting fringe capacitances, the metric (capacitance C) relating the voltage across the capacitor to the electrical displacement current through the capacitor is:

$$C = \frac{\varepsilon \cdot A}{t} \qquad \text{Eq. (3.1)}$$

where ε is the net dielectric permittivity of the polymer, A is the area of the overlap of the electrodes, and t is the distance between the electrodes. Equation (3.1) shows that the capacitance is directly proportional to the dielectric permittivity of the polymer and inversely proportional to the distance between the electrodes, which corresponds to the thickness of the polymer.

Upon exposing the sensor to a target analyte, two significant changes in the polymer's properties occur, relative to capacitance: (1) the polymer swells, and (2) the

dielectric permittivity, ε, increases. These changes are demonstrated in Fig. 3.1, which shows a capacitor without and with a target analyte present.

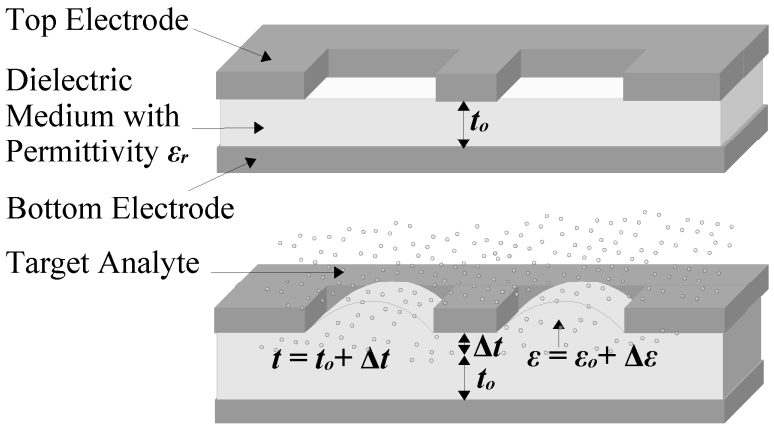

Figure 3.1. Parallel-plate capacitor with a polymer dielectric

Due to the opposite effects that swelling and a change in permittivity have on capacitance, as seen in Eq. 3.1, it is possible that the effects could offset each other. For example, if the dielectric permittivity increases by 10% and the polymer's thickness swells by 10%, no capacitive change would detectable. To avoid this scenario, the polymer must be chosen carefully so that swelling dominates the change in permittivity. While polymer selection is discussed in detail later in this chapter, an example of a good polymer to use for this sensor is one that absorbs low-permittivity analytes. The smaller the permittivity of the analyte is, the smaller the change in the polymer's net permittivity will be upon analyte absorption, thereby allowing swelling to dominate the response.

Key Design Decisions

Key design decisions that were made in an effort to implement the sensor were the selection of materials (electrode material and polymer) and the design of top electrode so that analytes would have access to the polymer and so that it would not impede polymer swelling. These topics are discussed in detail below.

Electrode Material Selection

Material for the electrodes was chosen based on the criteria of the material being a good electrical conductor and the ability to process the material. High electrical conductivity is important to minimize the series resistance of the sensor. Probable candidates were metal or degenerately-doped polysilicon. Due to the lack of polysilicon deposition capability at Boise State University, metal electrodes were chosen. As for processing the metal, it is desirable that the deposition and etching of the metal be uniform, reproducible, and have fast processing times. Uniformity of the processing is important in reproducing sensors with the same baseline capacitance.

Two concerns relative to metal selection are the delamination of the metal from the substrate and of the metal deposition and etching processes damaging the polymer. The bottom electrode (and pads for the top electrode) will be deposited on an insulating oxide. While delamination of the bottom electrode is of minimal concern, during operation of the sensor, the top electrode will push away from the substrate (oxide) as the polymer swells. Therefore, it is critical that the top electrode metal firmly adheres to the

oxide. Also, the chemicals, heat, and other processes required to deposit and etch the metal must not damage the polymer.

Because of the integration of fabrication processes (presented later in this chapter), different metals were chosen for the top and bottom electrodes. Titanium was chosen for the bottom electrode and aluminum for the top electrode. This was done because, at the end of the top electrode etch, the bottom electrode is exposed to the aluminum etchant. To prevent the bottom electrode from being etched at this time, a metal that resists aluminum etchant (titanium) is used.

Polymer Selection

Polymer selection is critical for the capacitance change of the sensor to be dominated by polymer swelling. Key issues pertaining to polymer selection are that:

- The polymer absorbs the desired analytes
- The polymer swelling is reversible when the target analyte is removed from the sensor
- The permittivity of the polymer be as large as possible relative to the target analyte
- The polymer is robust so that withstands sensor fabrication

These issues are described below.

The most critical property of the polymer from a senor functionality standpoint is that the polymer absorbs that target analyte. Methods to predict the absorption of

analytes by polymers have been reported (see Chapter 2: Literature Review for details and references). The caveat with these methods is that they require experimentally determined data. Therefore, if data pertaining to the specific polymer and analyte of interest are not reported in literature, extensive experiments must be done to obtain this data.

For repeated use of the sensor, the polymer swelling must be reversible so that the sensor returns to its baseline capacitance between analyte exposures. This typically requires that only weak bonds form between the polymer and analyte, such as van der waals or hydrogen bonding. If covalent bonds were to form between the analyte and polymer, much more energy would have to be applied to release the analyte from the polymer. A fundamental tradeoff exists between the reversibility and the selectivity of the polymer/analyte interactions. The lack of selectivity of polymer-based sensors has lead to the development of electronic noses, in which an array of different sensors is used and some form pattern recognition is implemented to better recognize specific analytes.

For this sensor, the permittivity of the polymer is an important property. Because this sensor relies on the swelling of the polymer, the permittivity of the polymer should be as large as possible relative to the permittivity of the analyte. Since the net permittivity always increases with the absorption of the analyte into the polymer, if the permittivity of the analyte is negligible to that of the polymer, the effects of the permittivity change are more likely to be negligible.

There are a few of processing concerns (any of which can render the polymer unusable) associated with the selected polymer.

- The polymer must be solid at temperatures at and above room temperature (that is, the glass transition or melting temperature of the polymer must be above room temperature). This is necessary so that metal can be deposited on the polymer. For example, experiments with the polymer polyisobutylene (PIB), which has a glass transition temperature that is lower than room temperature giving it a "tacky" property, showed that a 1μm-thick metal layer could not be deposited on the PIB. Because of the tacky and slightly liquid property of PIB, the metal tended to diffuse into the polymer so that there was no separation between the polymer and the metal. This rendered PIB useless for this sensor. However, experiments with polymers that have glass transition temperatures larger than 80°C (such as photoresist, PMMA, and poly(ethylene vinyl acetate) (PEVA)) showed that metal could be deposited on them.
- The polymer must sustain the etching process required to pattern the metal that is deposited on the polymer. Experiments to determine this must be done on a case-by-case basis.
- For this sensor the polymer must be able to be patterned (specific regions of the polymer must be able to be removed by etching it away). Plasma etching can remove many organic polymers, but the etch chemistries and other

processing parameters can vary widely from polymer to polymer. Also, if the polymer heats up beyond its glass transition temperature during the etch, the polymer can potentially flow, which is undesirable.

The polymer that was chosen to initially experiment with is poly(ethylene vinyl acetate) (PEVA). It was chosen because a literature search and lab experiments showed that it met all of the criteria listed above. PEVA has been shown to swell when exposed to toluene, octane and benzene (and de-swell when these analytes are removed). The dielectric permittivity all of these analytes is less than the permittivity of PEVA. Also, the adsorption of chemical warfare agent simulants dimethyl methylphosphonate (DMMP) and cholorethyl ether (CEE) have been reported [8]. Lastly, experiments in the Boise State University cleanroom showed that PEVA sustained a 50°C aluminum etch and that it could be plasma etched.

Top Electrode Design

The top electrode has two defining features. First, an array of holes must in the top electrode so that analytes can access the polymer. The size and spacing of these holes is potentially an important factor for optimizing the sensor's performance. Secondly, the top electrode must be able to flex away from the substrate when the polymer swells. Flexibility of the electrode is implemented by attaching the electrode to the substrate with

springs. Figure 3.2 shows a plan view drawing of a top electrode with access holes and springs.

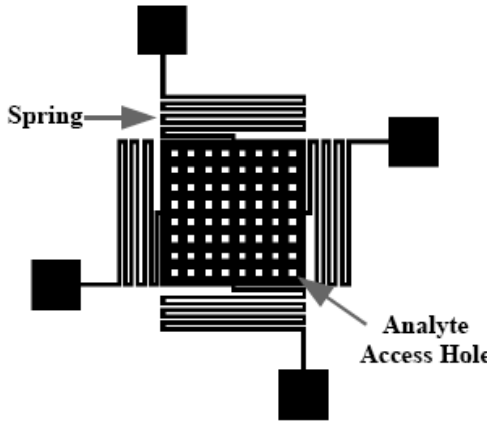

Figure 3.2. Plan-view drawing of top electrode with holes and springs

The flexibility of the springs is quantified by the spring constant. The larger the spring constant, the more flexible a spring is. Calculating a precise spring constant for this type of spring is complex. However, in general, the longer the spring, and the smaller the width, the larger the spring constant will be. Electrically, it is desired that the springs have low resistance (that they be highly conductive). Unfortunately, the physical properties that allow for a large spring constant, long length and small width, increase electrical resistance. Therefore, there is a tradeoff between the flexibility of the top electrode and the series resistance of the sensor. However, since the sensor is a capacitor, only small amounts of electrical current should be flow through it, so the series resistance likely will not be too concerning.

Process Integration

Process integration is the ordering of fabrication steps required to build something, in this case, the sensor. Desirable attributes of the process integration for the sensor is that it has the fewest steps necessary, uses low temperature processing (has small thermal budget), and that the processes be predictable and repeatable so that sensors from different batches have similar electrical characteristics. Designing a process integration scheme can be a complex task, as the designer must consider how the processes affect the performance of the device both electrically and mechanically.

Since the sensor is designed to be integrated with CMOS technology, the processing steps used to fabricate the sensor must not interfere with any CMOS devices that may eventually be integrated on the same wafer. The sensor would most efficiently be integrated with CMOS by placing the sensor on the back-end of the CMOS fabrication process, in the metal interconnect layers. This ensures that the complex, front-end-of-the-line CMOS transistor fabrication process does not have to be modified. The objective as far as integrating the sensor then would be to cause as little damage, perhaps thermal or contamination, to the circuitry as possible during sensor fabrication. One method of doing this might be to complete fabrication of the CMOS portion and pattern the bottom sensor electrode on the top layer of CMOS metal. Then passivate the circuit and etch openings to reveal the bottom electrode as well as a contact for the top electrode. The next section describes the sensor fabrication steps that are compatible with CMOS technology.

Process Flow

This section describes the theoretical ordering of steps to fabricate the sensor. Process parameters that are specific to the equipment used in the BSU cleanroom are postponed until Chapter 4, which describes the process development and simulation of the BSU equipment.

Bottom Electrode Module

The starting material is p-type, 1-10Ω-cm, (100) silicon wafers. The substrate type and doping for the sensor fabrication is not critical because the sensor is isolated from the substrate with oxide. A 5000Å isolation oxide is thermally grown, on which probe pads to both the bottom and top electrodes will rest. This thickness is chosen because the expected maximum voltage that will be applied to the sensors during testing is 1V. The approximate oxide breakdown voltage is 100V/μm, so 5000Å of oxide requires approximately 50V to be placed across it before it breaks down. As a side note, for a process that was integrated with CMOS, the insulating layer would be replaced by an inter-metal dielectric (IMD), which is typically a deposited oxide. Figure 3.3 shows a cross-section of the sensor after oxidation.

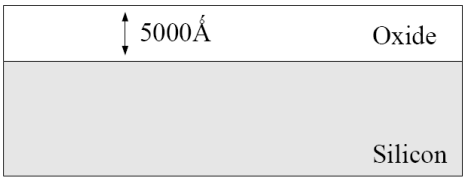

Figure 3.3. 5000Å of electrical isolation oxide.

The bottom electrode is made out of 2500Å titanium (shown in Fig. 3.4) because titanium is a conductive metal, is easily sputtered and etched, and resists aluminum etchant. The importance of it resisting aluminum etchant, as will be shown in a couple of steps, is because the top electrode (aluminum) rests on the same insulating oxide that the bottom electrode does, and making the bottom electrode out of a different metal allows the top electrode to be slightly over-etched without attacking or etching away the bottom electrode. To pattern the titanium, 1μm of photoresist is spun on the titanium and patterned using photolithography. The titanium is wet-etched using the photoresist as a hard mask. Wet etching is chosen (over dry etch) because it is selective to titanium and has short processing time. The resulting cross-section after bottom electrode patterning is shown in Fig. 3.5. The photoresist is removed using an acetone, IPA, methanol clean. Figure 3.6 is a 3-D (three-dimensional) drawing of the sensor after bottom electrode module fabrication.

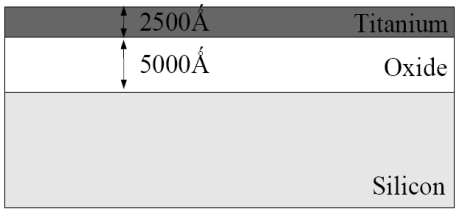

Figure 3.4. 2500Å of titanium for the bottom electrode

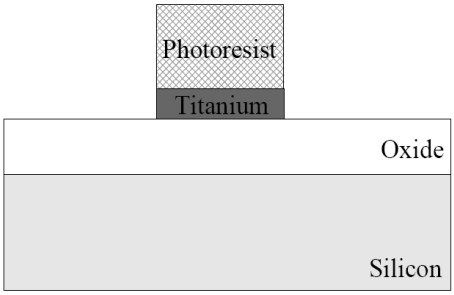

Figure 3.5. Patterning and etching of the titanium electrode.

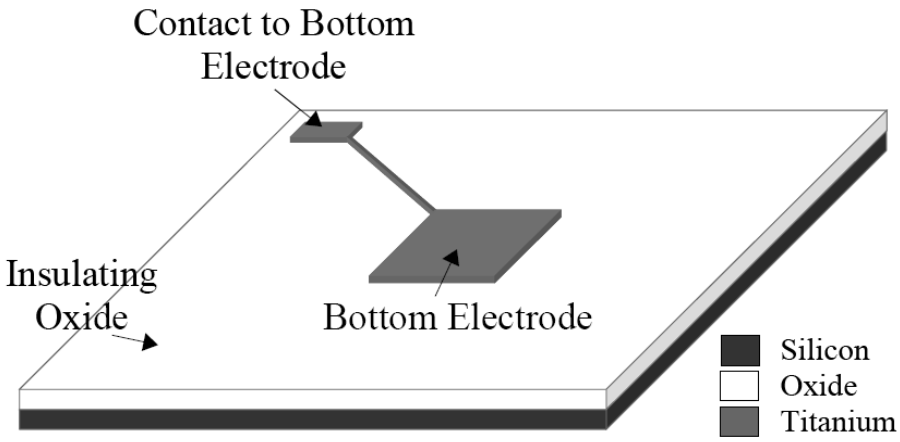

Figure 3.6. 3-D drawing of the sensor after bottom electrode fabrication

Polymer Dielectric Module

Polymer Application

Poly(ethylene vinyl acetate), or PEVA, is used as the chemically sensitive dielectric layer. It is spun on with a spin coater at a target thickness of 1μm, as shown in Fig. 3.7. Thinning at the corners of the electrode is a concern because the thinner the polymer is, the more likely it is that the sensor will breakdown in that region. However, the polymer is four times thicker than the bottom electrode metal, so this should be sufficiently thick. A solvent bake-out will be necessary to harden the PEVA.

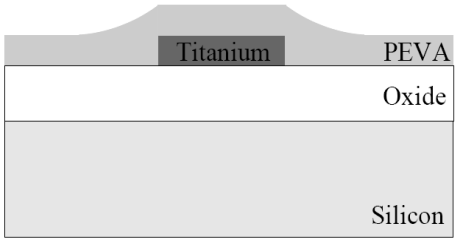

Figure 3.7. PEVA application by spin-coating

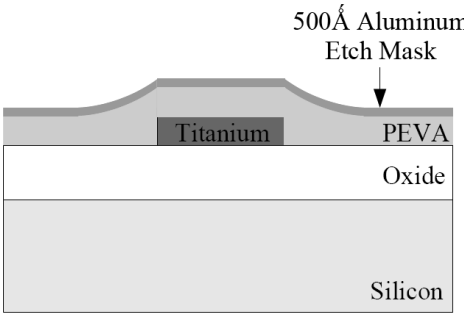

Figure 3.8. Aluminum hard mask deposition

Polymer Patterning

The PEVA is patterned by plasma etching. To accomplish this, a 500Å aluminum hard mask is sputtered on the PEVA, as shown in Fig. 3.8. The mask is patterned using photolithography and wet etching of the aluminum, as shown in Fig. 3.9. Photoresist on the aluminum is removed with an acetone, IPA, methanol clean. This clean does not remove the PEVA. The PEVA is plasma etched in a barrel asher using O_2 and CF_4 chemistry. The etch chemistry does not attack the aluminum hard mask, so after the etch, PEVA will remain in all areas that are covered by aluminum (Fig. 3.10). Finally, the aluminum mask is removed with wet etching, as shown in Fig. 3.11. At this point a substantial hard bake is done to harden the

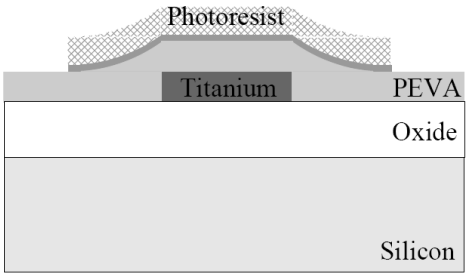

Figure 3.9. Pattern hard mask

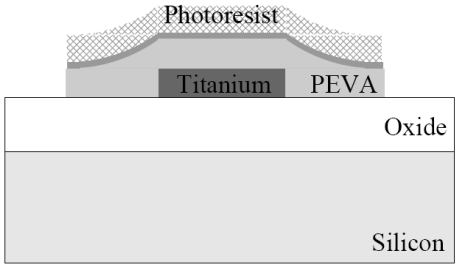

Figure 3.10. Plasma etching of PEVA

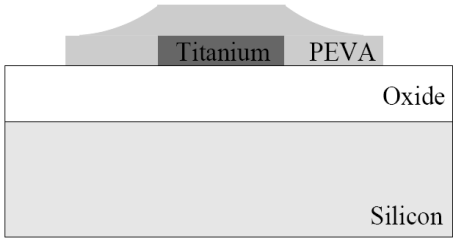

Figure 3.11. Removal of hard mask

PEVA even further so that is robust enough to withstand the subsequent aluminum etch for the top electrode. Figure 3.12 is a 3-D drawing of the sensor after the polymer dielectric module fabrication.

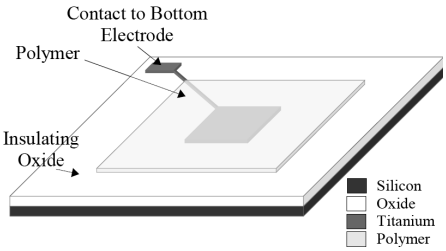

Figure 3.12. 3-D Drawing of sensor after PEVA patterning

Top Electrode Module

2500Å of aluminum is used for the top electrode, as shown in Fig. 3.13. Photoresist is spun on the aluminum and is patterned with photolithography. The aluminum is wet-etched, as shown in Fig. 3.14. Lastly, the photoresist is removed with an acetone, IPA, methanol clean.

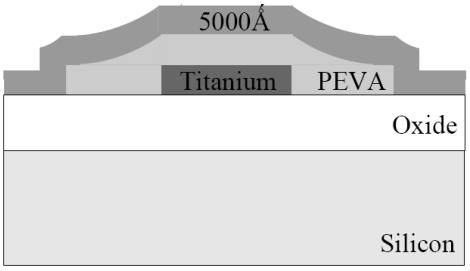

Figure 3.13. 2500Å of aluminum for the top electrode

This is the final step in the process flow. Figure 3.15 shows a 3-D drawing of the completed sensor after the top electrode module fabrication.

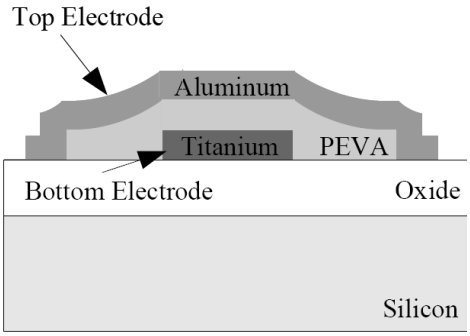

Figure 3.14. Patterning of the top electrode

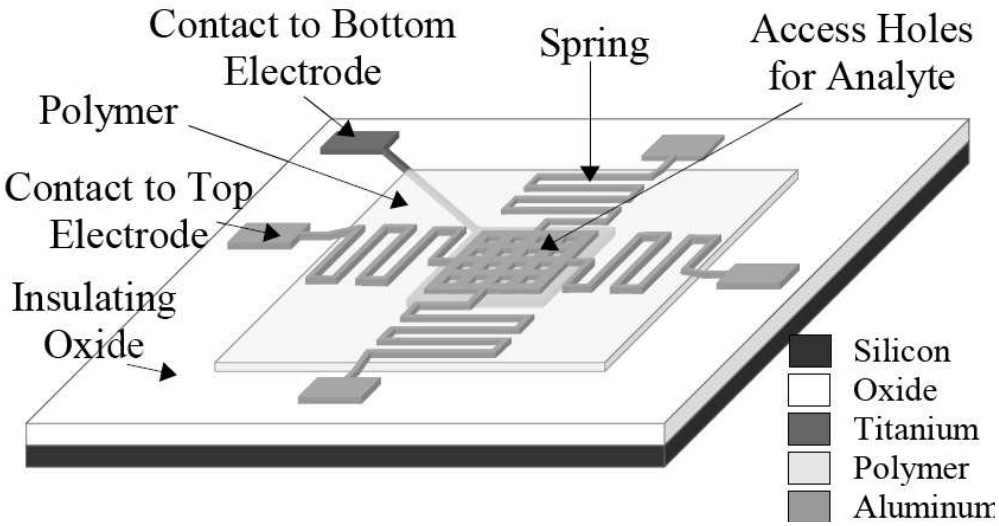

Figure 3.15. 3-D drawing of the sensor after top electrode fabrication

This proposed process flow is compatible with CMOS technology. It does not require any significant thermal steps, and provided that the CMOS circuitry is passivated prior to sensor fabrication, it is expected that very little contamination would occur as none of the materials, such as the polymer, would come in physical contact with any transistors.

Photolithography Mask Design

The general shapes of the different layers (for example, the electrodes or PEVA layer) are defined using photolithography. Photolithography requires the use of masks. A mask is a thin piece of quartz or soda lime that is coated with chrome. The chrome is etched to yield the desired shapes and their polarities (transparent or opaque). A mask is then used like a stencil to transfer the pattern many times onto substrates using photolithography.

A mask set was designed to enable the proposed process flow to be implemented. The process flow is relatively simple, as it only requires three photolithography steps. If the masks for this process flow are designed correctly, no critical photolithography alignment steps will be necessary (that is, some error in alignment is tolerable and should not drastically effect the sensor operation).

A die with various sensor features was laid out on the masks. The die was reproduced thirteen times on masks, which were designed for use with four-inch diameter wafers. The general layout of a single die is shown in Fig. 3.16.

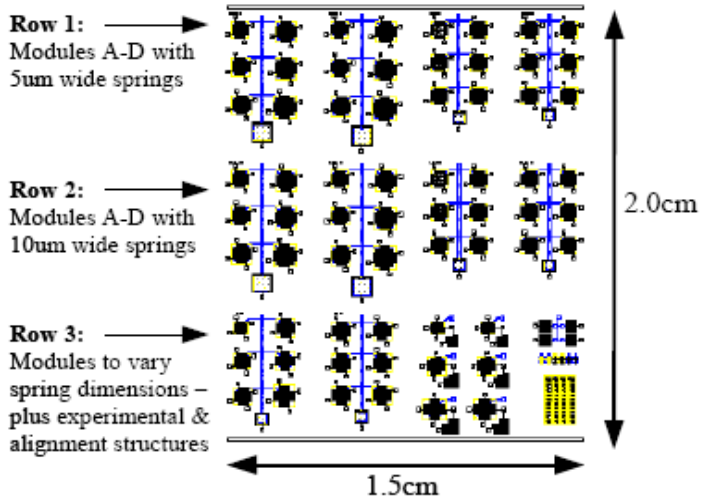

Figure 3.16. Die layout from photolithography mask set

The various modules seen in Fig. 3.16 were systematically set up to vary critical parameters of the sensor, these being access hole size, density, and spring dimensions. Module A and B contain capacitors with varying areas. Module A varies the number of holes that are used (with fixed hole size and spacing between holes), while Module B varies the distance between the holes (with fixed hole size and number of holes). The specific parameters are described in Table 3.1.

Table 3.1. Top Electrode Hole Size and Spacing for Varying Capacitor Dimensions

Name	Variable	Hole Dimensions (µm x µm)	Hole Spacing (µm)	# of Holes	Capacitor Dimensions (µm x µm)
Module A	# of Holes	10 x 10	20	14	440 x 440
		10 x 10	20	16	500 x 500
		10 x 10	20	18	560 x 560
		10 x 10	20	20	620 x 620
		10 x 10	20	22	680 x 680
		10 x 10	20	24	740 x 740
Module B	Hole Spacing	10 x 10	30	10	430 x 430
		10 x 10	35	10	485 x 485
		10 x 10	40	10	540 x 540
		10 x 10	45	10	595 x 595
		10 x 10	50	10	650 x 650
		10 x 10	55	10	705 x 705

Module C and D contain capacitors with fixed areas. Module C varies both the number of holes and the spacing between the holes (with fixed hole size and capacitor area). Module D varies the distance between the holes and the size of the holes (with

fixed number of holes and capacitor dimensions). The specific parameters are described in Table 3.2.

Table 3.2. Top Electrode Hole Size and Spacing for Fixed Capacitor Dimensions

Name	Variable	Hole Dimensions (µm x µm)	Hole Spacing (µm)	# of Holes	Capacitor Dimensions (µm x µm)
Module C	# of holes Hole Spacing	10 x 10	143	14	450 x 450
		10 x 10	82	16	450 x 450
		10 x 10	56	18	450 x 450
		10 x 10	41	20	450 x 450
		10 x 10	32	22	450 x 450
		10 x 10	25.5	24	450 x 450
Module D	Hole Spacing Hole Size	2.5 x 2.5	48	8	450 x 450
		5 x 5	45.5	8	450 x 450
		10 x 10	41	8	450 x 450
		15 x 15	36.5	8	450 x 450
		20 x 20	32	8	450 x 450
		25 x 25	28	8	450 x 450

Modules A-D were laid out with springs that were both 5μm and 10μm wide. Figure 3.17 shows a schematic of a spring and how the dimensions are defined.

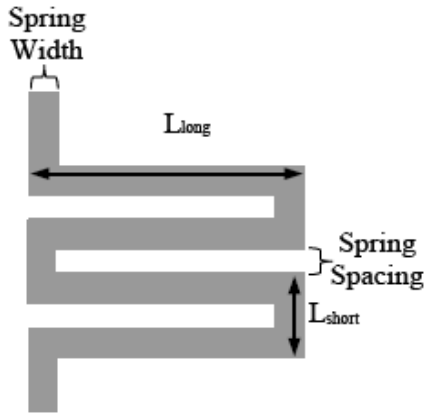

Figure 3.17. Spring parameters

Variations of these spring dimensions were included in the third row on the die, as seen in Fig. 3.16.

Summary

This chapter presented the conceptual design of the sensor and described its theoretical operation. A discussion of which materials would be used and why was included. A process integration scheme was presented and the design of the photolithography masks needed to fabricate the sensor was detailed.

CHAPTER 4: PROCESS DEVELOPMENT & PROCESS SIMULATION

Preparation prior to sensor fabrication was critical for saving time and money. Each fabrication process that needed to be used characterized, and an understanding of how the processes would interact with each other was thought out as well. Specifically, the tasks of oxidation, 1μm resolution photolithography, the deposition and etching aluminum and titanium, and application and patterning of PEVA were characterized by performing lab experiments. In addition to this characterization, many of the processes were modeled using Silvaco Athena and Tonyplot [43], a process simulation software tool. Modeling can allow for the investigation of process changes without performing costly, experimental fabrication. Lastly, the entire sensor fabrication was simulated with Silvaco Athena. The details of these topics are presented in the following sections.

Process Development of BSU Cleanroom Tools

Oxidation

Silicon dioxide (oxide) is a relatively good electrical insulator and is relatively simple to grow on a wafer. To grow an oxide, a silicon wafer is placed in a hot furnace (800-1200°C) and is exposed to an oxidizing agent(s). Two common thermal oxidation

processes are dry oxidation and wet oxidation. They are differentiated by the oxidizing agents used to grow them, and grow at different rates, producing different qualities of oxides. Dry oxide is generally of higher quality that wet oxide, but takes a considerably longer time to grow (especially for thick oxides, which render dry oxidation impractical).

Oxidation growth can be modeled with the Deal-Grove Model, which provides the following equation relating the final oxide thickness (t_{ox}), initial oxide thickness (t_o), and time (t) given in Eq. 4.1:

$$t_{ox}^{\,2} + A \cdot t_{ox} = B \cdot \left(t + \frac{t_o^{\,2} + A \cdot t_o}{B} \right) \qquad \text{Eq. 4.1}$$

A and B are strongly dependent on temperature, which has large effect on growth rate. The Deal-Grove model is accurate for oxides thicker that a few hundred angstroms.

A Minibrute oxidation/diffusion furnace was used to perform oxidation growth for the sensor. A series of data sets consisting of time, temperature, and thickness for ten runs was collected and the data was used to back-solve for the coefficients B/A and B in Eq. 4.1 (when 6sccm of O_2 flow into furnace during oxidation). These coefficients, which are functions of temperature (T), are listed below:

$$\left(\frac{B}{A}\right)_{wet,(100)} = \left(7.14\times10^{7}\ \frac{\mu m}{hr}\right)\exp\left(\frac{-2.05}{(8.62\times10^{-5})(T)}\right)$$

$$\left(\frac{B}{A}\right)_{dry,(100)} = \left(3.71\times10^{6}\ \frac{\mu m}{hr}\right)\exp\left(\frac{-2.00}{(8.62\times10^{-5})(T)}\right)$$

$$(B)_{wet,(100)} = \left(350\frac{\mu m^{2}}{hr}\right)\exp\left(\frac{-0.71}{(8.62\times10^{-5})(T)}\right)$$

$$(B)_{dry,(100)} = \left(772\frac{\mu m^{2}}{hr}\right)\exp\left(\frac{-1.23}{(8.62\times10^{-5})(T)}\right)$$

With these functions, the time to grow a required oxide thickness can be determined (given the silicon crystal orientation, wet or dry method to be used, and initial oxide thickness). To grow a 5000Å oxide in the BSU cleanroom at 1100°C, wet oxidation takes 31 minutes, whereas dry oxidation takes 13.5 hours.

Photolithography

Photolithography is a method to transfer patterns (sub-micron and larger) onto a wafer. A simple photolithography process involves priming the wafer (cleaning), then spinning photoresist on the wafer, followed by a soft bake to harden the resist. Exposing the resist to ultraviolet light (UV) causes a chemical reaction to occur. For example, if positive-tone photoresist is used, the UV light breaks apart cross-linked polymer chains in the resist. A wet chemical solution called developer removes the areas of the resist where the chains have been broken apart. To create a pattern with this method, a mask (with clear and opaque features on it) is placed on (or near) the surface of a photoresist-

coated wafer. The UV light shines through the clear regions of the mask and is reflected by the opaque features on the mask. Therefore, the pattern on the mask is transferred to the photoresist.

Photolithography in the BSU cleanroom requires six steps: HMDS cleaning, resist spin-on, soft-bake, resist exposure, developing, and hard-bake. The first step is to prime the wafer with HMDS (a cleaner) by spinning the wafer at a high speed on the spin coater and dispensing ~ ½ mL of HMDS on the wafer. Specific details (time, spin speed, and ramp rates) for the Headway Research Inc. Spin Coater recipes for HMDS and photoresist are shown in Table 4.1. Immediately following the HMDS, 1mL of photoresist is dispensed on the wafer.

Table 4.1. HMDS and Resist Spin Coater Recipes

	Step 1			**Step 2**		
Material	**Time (sec)**	**Speed (RPM)**	**Ramp (RPM/sec)**	**Time (sec)**	**Speed (RPM)**	**Ramp (RPM/sec)**
HMDS	5	500	1000	35	5000	1000
1μm-thick photoresist (SPR 220-1.2)	30	3500	2000	0	0	0

The thickness of the photoresist is measured with a NanoSpec Film Measurement System. A soft-bake, used to bake-out some of the solvents in the resist, is done on a hot-

plate. For the 1μm resist recipe in Table 4.1, a soft bake of 1 minute at 90°C is typically used. After cooling from this bake, the resist is exposed. A Quintel Contact Aligner is used both to align the mask to pre-existing features on the wafer and as a source of UV light to expose the resist. For the alignment portion of this task, the wafer is place on a vacuum chuck and is brought very close to the surface of the mask. Alignment is done manually and can have accuracy of around 1μm. Once properly aligned, the mask and wafer (coated with photoresist) are brought into contact with each other. Upon exposure, this method will yield a 1:1 transfer of pattern; that is, the pattern on the mask will be the same size as that transferred into the photoresist. This is in contrast to some systems that use a mask with features larger than desired, which are then optically reduced during exposure. Once the mask and wafer are in contact with each other, UV light is used to expose the resist. The user sets the time of exposure based on the intensity of the light. This must be experimentally determined. If the image is over-exposed (too much time for the given intensity), the pattern will be too large (over-exposed) and squared corners will round off. If under-exposed, residual resist will remain after developing, which will affect the processing following patterning. The parameters that were developed for the BSU contact aligner are shown in Table 4.2.

Table 4.2. Contact Aligner Parameters for 1μm Feature Photolithography

Resist Thickness	**Smallest Mask Feature**	**Measured UV Intensity**	**Exposure Time**
1μm	1μm	11.5mW/cm^2	2 seconds

After exposure with the contact aligner, the resist is chemically developed. Development is performed in a beaker under hood at wetsink. At room temperature, the experimentally determined development time is about 1 minute, but varies depending on how many times the developer has been used. The wafer is immediately transferred to a beaker of DI water after development in order to stop the development process. After a 30 second rinse in the beaker, the wafer is gently sprayed with DI water for another 30 seconds and is then dried with a pressurized air hose. Pattern fidelity is inspected in an optical microscope after development. If the pattern is not sufficient, in most cases, the photoresist can be removed with an acetone, IPA, and methanol clean or with photoresist stripper. If the pattern is sufficient, generally a hard bake is performed in order to make the resist more robust to the next processing step, which is almost always an etch step. The hard bake recipe that is commonly used in the cleanroom is a 2-minute bake at 160°C in a convection oven.

Metal Deposition

Two common methods of metal deposition are chemical-vapor-deposition (CVD) and physical sputtering. CVD is done in a vacuum chamber in which specific gases are introduced into the chamber and involves a chemical reaction that occurs on the surface of the wafer. Because of this surface reaction, CVD can provide excellent step coverage, meaning that the deposited film thickness is relatively uniform on all surfaces regardless of what angle the surface is parallel to the substrate (such as parallel or perpendicular). Physical sputtering is also performed in a vacuum chamber. Here, a process gas, usually argon flows into the chamber. A voltage (DC or RF) is applied between the grounded anode, where the wafer is placed, and a powered electrode where a piece of metal (target) that will be sputtered is placed. The applied voltage ionizes the argon and the ions are electrical accelerated towards the target. They collide with the target and dislodge metal molecules. The molecules fill the chamber and deposit on the wafer (as well as most other portions of the chamber)

At the time of fabrication, the only reliable method of metal deposition at BSU was with a CrC 150 Sputter System. Step coverage was a concern with this tool because it uses sputtering and not surface chemical reactions (CVD). The required metals for the sensor were aluminum and titanium. The deposition rates for these metals for the CrC are shown in Table 4.3.

Table 4.3. CrC Metal Deposition Rates

Metal	Process Gas	Process Pressure	DC Power	Deposition Rate Å/min	Deposition Rate µm/hr
Aluminum	Argon	5 mTorr	50 W	70	0.42
Titanium	Argon	5 mTorr	50 W	33	0.2

Metal Etching

There are two general categories of etching metals, dry and wet. Dry etching involves placing the metal-coated wafer in a vacuum chamber and using either chemicals to etch the metal, or to bombard the wafer with ionized molecules (or some combination of the chemical and bombardment processes). Dry etching can either be anisotropic or isotropic, although usually a very directional, anisotropic etch is desired to yield vertical sidewalls on the metal features. Wet etching is done in liquid chemicals. In general, it is used less often than dry etching due to the difficulty of controlling the process and the potential contamination. However, wet etches can be very selective.

At the time of fabrication, only wet etching was available at BSU. Table 4.4 shows the etch rates for aluminum and titanium. The rates were determined by patterning the metal with photolithography, etching for a specified period of time (using the resist as a mask), and then measuring the step height with a SEM.

Table 4.4. Metal Wet Etch Rates

Metal	**Etch Chemistry**		**Temperature**	Rate (Å/min)
Aluminum	Phosphoric Acid (85%) Nitric Acid (70%) Acetic Acid (99.7%) DI Water	16 parts 1 part 1 part 2 parts	50°C	6500
Titanium	Hydrofluoric Acid (49%) Hydrogen Peroxide DI water	1 part 1 part 20 parts	Room Temperature	8500

PEVA Application and Etching

Many of the chemically selective polymers used for chemical sensors are not commonly used materials in the micro-fabrication industry and therefore do not have well-developed processes to pattern and etch them. General methods of applying polymers are to use spin-coating or spray-coating. Typically, organic polymers can be plasma etched using oxygen, although the etch rates can be slow. To enhance the etch rate, a ratio of approximately 80% CF_4 to 20% O_2 can be used. The chemical composition of the gases and etch rates vary greatly for different types of polymers. Heat treatment of polymers prior to etching can harden the polymers and make them more difficult to etch.

As described in Chapter 3, the polymer that was to be used for the sensors is PEVA. No processes to pattern PEVA were found in literature, so an in-house process was developed. PEVA is purchased in solid pellet form, and therefore had to be dissolved into liquid form so that it could be spun on a wafer. 5 grams of PEVA pellets were dissolved into 80mL of toluene. To assist dissolving, the solution was heated to 50°C on a hotplate and stirred for 30 minutes under a fume hood. NOTE – toluene is very explosive, so extreme caution was taken at this step. The liquid PEVA was spun onto a wafer using the spin coater. 1mL of PEVA was dispensed with a disposable dropper and was then spun for 30 seconds at 3500RPM. Next, a 5-minute solvent bake-out at 75°C on a hotplate was performed. 75°C was chosen because it is slightly under the glass transition temperature of PEVA (exceeding the glass transition temperature could cause the PEVA to run). The film thickness was measured with a NanoSpec Film Thickness Measurement System and yielded a thickness of approximately 1μm (with the index of refraction (Nf) = 1.46).

To pattern the PEVA, a metal etch mask was used. An aluminum mask was used because titanium caused the PEVA to crack. 500Å of aluminum was deposited on the PEVA in the CrC Sputter System (power=50W; time=8 minutes; process pressure=5mTorr). The aluminum was patterned with standard photolithography. However, in effort to not exceed the glass transition temperature of PEVA, a 1-minute 30-second soft-bake (pre-exposure) at 75°C was used and a 4-minute hard bake (post develop) at 75°C was done. These lower temperature bakes (relative to the typical 90°C

soft bake and 160°C hard bake) did not noticeably affect the integrity of the pattern (minimum feature size was 2μm). After hard baking the resist, the aluminum was wet-etched down to the underlying PEVA. Finally, the photoresist on the remaining aluminum features was removed using an acetone, IPA, and methanol rinse (30 seconds with each). The PEVA was resistant to this solvent clean.

With the aluminum hard mask in place, the PEVA was etched in a Branson plasma barrel etcher. The chemistry used for the etch was 80sccm of CF_4 and 20sccm of O_2. While O_2 is often used to descum organic polymers, the addition of the CF_4 greatly enhances the etch rate. The etch parameters were 50W (RF forward power) and process pressure of 500mTorr. The etch rate was approximately 0.22μm/min. Therefore, the time to etch a 1μmthick film was 4 minutes and 30 seconds. However, a 20% over-etch was employed, so the total etching time was 5 minutes and 30 seconds.

Simulation of BSU Fabrication Processes

Oxidation

Silvaco Athena was used to model the oxidation characteristics of the Minibrute furnace. To tune the simulator, the pressure parameter was modified (even though the real pressure may not be the same as what is in the code, the temperature and time will be close). The following is Silvaco Athena syntax to grow 5000Å of oxide using wet oxidation (Fig. 4.1):

```
go athena
line y loc=0  spac=0.2
line y loc=1  spac=0.2
line x loc=-1   spac=0.2
line x loc=1    spac=0.2
init silicon c.boron=3e14 orient=100
diffuse time=82 temp=1000 weto2
 #Tune with press parameter
press=.93
structure outfile=oxidation.str
tonyplot -str oxidation.str
quit
```

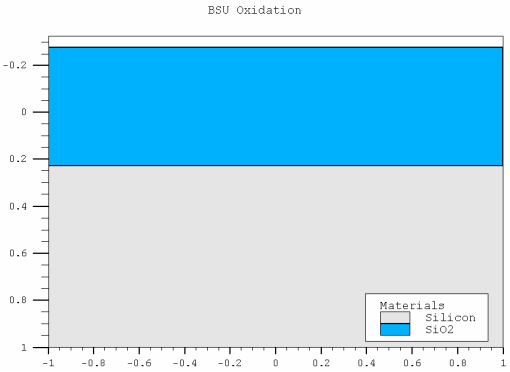

Figure 4.1. Minibrute oxidation simulation

Metal Deposition

The CrC-150 Sputtering System was used to deposit metal. Silvaco code to model aluminum deposition with a rate of 4000Å/hr (50W, 500mTorr) is:

```
go athena
diffuse time=82 temp=1000 weto2
press=.9
```

```
etch oxide right p1.x=0
rate.depo machine=CrC aluminum u.h
unidirec dep.rate=.4 angle1=0
deposit machine=CrC time=1 hours
divisions=10
structure outfile=aluminum.str
tonyplot -str aluminum.str
```

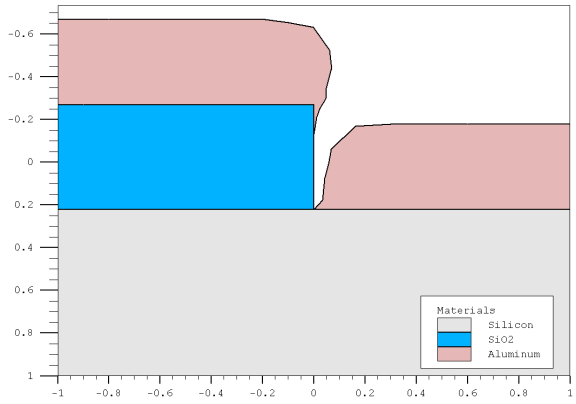

Figure 4.2. CrC aluminum deposition simulation

Code to model titanium deposition with a rate of 2000Å/hr (50W, 500mTorr) is:

```
go athena
diffuse time=82 temp=1000 weto2 press=.9
etch oxide right p1.x=0
rate.depo machine=CrC titanium u.h unidirec dep.rate=.2 angle1=0
deposit machine=CrC time=1 hours divisions=10
structure outfile=titanium.str
tonyplot -str titanium.str
```

These simulations show that metal deposited on materials with vertical sidewalls will likely be discontinuous. Therefore vertical sidewalls need to be avoided in the process integration.

Metal Etching

Aluminum wet etch is 6500Å/min at 50°C using etch solution in Table 4.3. The code to model this is:

```
go athena
rate.depo machine=CrC aluminum
u.h unidirec dep.rate=.42 angle1=0
deposit machine=CrC time=2 hours
divisions=10
deposit photoresist thick=.25
etch photoresist right p1.x=.45
#AL etch rate at 50C
rate.etch machine=wet_AL_etch
aluminum a.m  wet.etch iso=6500
etch mach=wet_AL_etch  time=1.3
minute dx.mult=.05
structure outfile=aluminum_etch.str
tonyplot -str aluminum_etch.str
quit
```

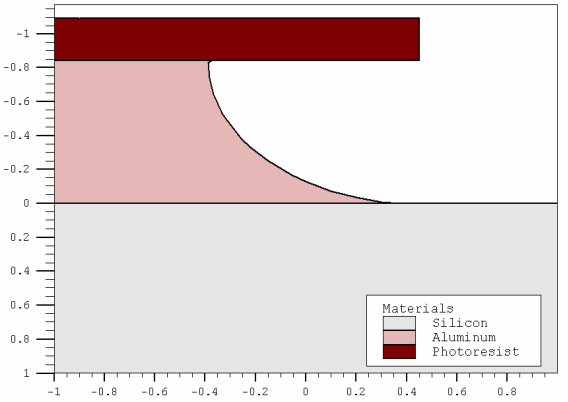

Figure 4.3. Aluminum wet etch simulation

The etch profile is shown in Fig. 4.3. Because wet etches are very isotropic, the aluminum etches almost the same amount in lateral and vertical directions.

Titanium wet etch is 8500Å/min at 22°C using etch solution in Table 4.4. Titanium is modeled using that same code, but the rate.etch statement is slightly different. It is listed below:

rate.etch machine=wet_Ti_etch titanium a.m wet.etch iso=8500

PEVA Etching

An image of the PEVA etch profile, when etched in the Branson Barrel Etcher, is shown in Fig. 4.4.

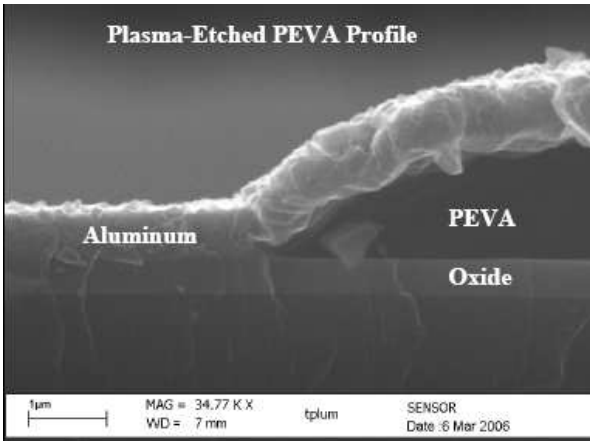

Figure 4.4. SEM image of PEVA etched in the Branson barrel etcher

The profile is rounded and has been observed on PMMA and nitride films that have been etched with this tool. Modeling of this profile in Silvaco was not achievable. In order to model the subsequent sensor fabrication, a simple angled etch will be used.

Simulation of Sensor Fabrication

This section provides the complete Silvaco Athena code to simulate the fabrication of the Bottom Electrode Module, Polymer Dielectric Module, and Top Electrode Module.

Simulation of Bottom Electrode Module

Below is annotated Silvaco Athena syntax to model the Bottom Electrode Module.

```
go athena
        #Define grid
line y loc=0  spac=0.1
line y loc=2  spac=1
line x loc=0  spac=0.1
line x loc=22.5 spac=0.1
        #Define basic silicon parameters.
init silicon c.boron=3e14 orient=100
        #Define machines that will be used in fabrication
rate.depo machine=PR_deposit photoresist  u.m  cvd dep.rate=1 step.cov=.1
smooth.win=.1 smooth.step=10
```

```
rate.depo machine=PEVA_Spin photoresist name.res=PEVA u.m cvd
dep.rate=1.0 step.cov=1.0 smooth.win=1 smooth.step=1

rate.depo machine=CrC_AL aluminum u.h unidirec dep.rate=.4 angle1=0
rate.depo machine=CrC_Ti titanium u.h unidirec dep.rate=.2 angle1=0
rate.etch machine=wet_AL_etch aluminum a.m  wet.etch iso=6500
rate.etch machine=wet_Ti_etch titanium a.m  wet.etch iso=8500

######## Bottom Electrode Module ############
        #Step 1: grow insulating oxide in Minibrute furnace
diffuse time=82 temp=1000 weto2 press=.93
        #Step 2: deposit 2500A of titanium in CrC Sputter Tool
deposit machine=CrC_Ti time=1.25 hour divisions=5
        #Step 3: Photolithography with bottom electrode mask
deposit machine=PR_deposit time=1 divisions=10
etch photoresist right p1.x=8
        #Step 4: Wet etch titanium bottom electrode
etch mach=wet_Ti_etch time=.33 minute dx.mult=.1
etch photoresist all
structure outfile=bottom_electrode.str
tonyplot bottom_electrode.str
```

Figure 4.5 shows the resulting structure from the code above.

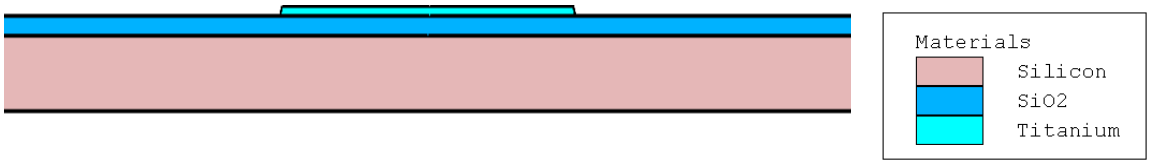

Figure 4.5. Simulation of bottom electrode module

Simulation of Polymer Dielectric Module

Continuing from the code above, the syntax to model the PEVA processing is below.

```
############ PEVA Dielectric Module ##############
        #Step 1: spin on 1um of PEVA using spin coater
deposit machine=PEVA_Spin time=1 minute divisions=20
        #Step 2: Sputter 500A aluminum on PEVA to serve as hard mask
deposit machine=CrC_AL time=.125 hours divisions=5
        #Step 3: Pattern aluminum etch mask using photolithography
etch aluminum right p1.x=21
        #Step 4: PEVA etch model - unable to accurately model barrel etcher
        #Therefore will use a simple angled etch that resembles real profile
etch material=PEVA thick=1 angle=50
        #Remove aluminum etch mask
```

etch aluminum all

structure outfile=PEVA_Etch.str

tonyplot PEVA_Etch.str

Figure 4.6 shows the resulting structure up to the PEVA patterning.

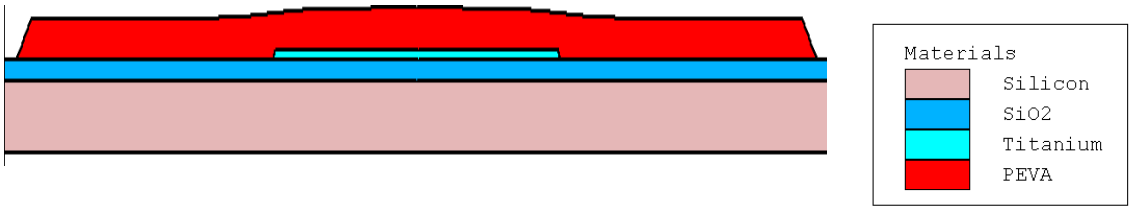

Figure 4.6. Simulation of polymer dielectric module

Simulation of Top Electrode Module

The code below completes the sensor fabrication modeling.

############ Top Electrode Model ###############

#Step 1: Deposit 2500A of aluminum with CrC for top electrode

deposit machine=CrC_AL time=.625 hour divisions=20

#Step 2: Pattern top electrode using photolithography

deposit photoresist thick=1 divisions=1

#access hole 1

etch photoresist start x=0 y=0

```
etch      cont  x=0 y=-3

etch      cont  x=1 y=-3

etch      done  x=1 y=0

          #access hole 2

etch photoresist start x=3 y=0

etch      cont  x=3 y=-3

etch      cont  x=5 y=-3

etch      done  x=5 y=0

          #Right Spring 1

etch photoresist start x=9 y=0

etch      cont  x=9 y=-3

etch      cont  x=11 y=-3

etch      done  x=11 y=0

          #Right Spring 2

etch photoresist start x=12 y=0

etch      cont  x=12 y=-3

etch      cont  x=14 y=-3

etch      done  x=14 y=0

          #Right Spring 3

etch photoresist start x=15 y=0

etch      cont  x=15 y=-3
```

```
etch      cont  x=17 y=-3
etch      done  x=17 y=0
          #Right Spring 4
etch photoresist start x=18 y=0
etch      cont  x=18 y=-3
etch      cont  x=20 y=-3
etch      done  x=20 y=0
structure outfile=top_elec_resist.str
          #Step 3: Wet etch top electrode aluminum
etch mach=wet_AL_etch time=.385 minute dx.mult=.09
          #Step 4: Remove photoresist
etch photoresist all
struct mirror left
structure outfile=top_electrode.str
tonyplot top_electrode.str
quit
```

Figure 4.7 shows the complete modeled sensor.

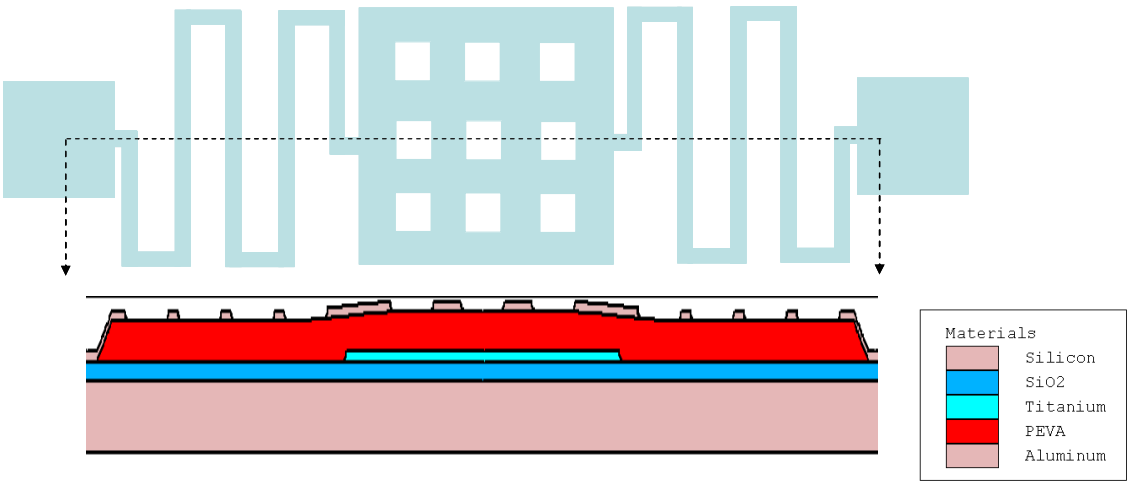

Figure 4.7. Simulation of top electrode module

Summary

This chapter presented the groundwork that was done prior to sensor fabrication, including characterization of the individual fabrication processes and simulation of the processes and entire fabrication sequence.

CHAPTER 5: SENSOR FABRICATION

This chapter provides a detailed description of the fabrication of the sensor. A brief mentioning of why specific materials are used is included; however, Chapter 3 provides in-depth discussions of why materials were chosen. Also, tools and parameters used to perform the fabrication are listed. Finally, any mentioning of the "cleanroom" is referring to the Idaho Microfabrication Laboratory at Boise State University.

Standard Processes:

Because some of the processes are used multiple times during sensor fabrication, they will be described once in detail here and then just referred to for the remaining chapter. The standard processes are 1μm photolithography, photoresist removal, and wet aluminum etch.

- Standard 1μm Photolithography: 1μm of photoresist (SPR-220 1.2) is spun on a wafer using the spin coater (3500RPM for 30 seconds). The resist is then soft-baked, but due to the various materials used, the soft-bake time and temperature will vary and will be specified at the particular processing step. The resist is then exposed using the contact aligner in the cleanroom. The optimal exposure for the

resist is 2 seconds at a dose of 11.5mW/cm^2. The resist is then developed for approximately 1 minute (depending on how many times the developer had been previously used). Finally, the resist is hard-baked. Again though, due to the various materials used, the hard-bake time and temperature will vary and will be specified at the particular processing step

- Standard Photoresist Removal: The standard photoresist removal process is to rinse the wafer with acetone (30 seconds), IPA (30 seconds), and finally methanol (30 seconds). The wafer is then dried with compressed air.
- Standard Aluminum Etch: The standard aluminum etch used a wet chemistry of 16 parts Phosphoric Acid (85%), 1 part nitric acid (70%), 1 part acetic acid (99.7%), and 2 parts DI water. The etch rate of this chemistry for aluminum deposited with the CrC sputter system is 6500Å/min at 50°C.

Bottom Electrode Module

The bottom electrode module spans from bare silicon to the patterning of the bottom electrode. The steps to fabricate this module are:

- **Thermal Oxidation**. Oxide serves as the electrical insulator between the silicon substrate and the bottom electrode. Also, the pads for the top electrode will land this oxide. 5000Å is sufficiently thick, as the sensors will be tested with an LCR meter using a 1V testing voltage. Since the breakdown voltage of oxide is ~100V/um, an ideal oxide of 5000Å could sustain up to 50V. The oxide was

grown in the Minibrute oxidation furnace in the cleanroom. Wet oxidation was used in order to enhance the growth rate. The oxidation took 82 minutes at 1000°C while flowing 6sccm of O_2 through a bubbler (with water at 98°C) into the furnace tube.

- **Titanium Deposition**. Following the oxidation, 2500Å of titanium was deposited for the bottom electrode metal. Titanium was used so that the aluminum etching for the top electrode would not etch the bottom electrode (as the bottom and top electrode both rest on the same oxide layer). The resistance of the metal was not a major concern because not much current will be flowing through the capacitor and the wires connecting to the electrodes were 50μm wide (relatively wide – the wider, the smaller the resistance). The titanium was deposited using the CrC Sputter System in the cleanroom. The deposition took 75 minutes at a DC power of 50W and a process pressure of 5mTorr (using argon as the ionizing gas). Due to the slow deposition rate of titanium, a thin film of metal was desired simply for shorter processing time.
- **Titanium Pattern and Etch**. To pattern the titanium, photolithography and wet etch were used. The standard 1μm photolithography process was used to pattern resist on the titanium using the bottom electrode mask. A pre-exposure soft-bake of 90°C for 1 minute was used. After passing a post-developing visual inspection of the resist pattern, the resist was hard-baked at 160°C for 2 minutes in a convection oven. The titanium was etched with hydrofluoric acid (49%),

hydrogen peroxide, and DI water (1:1:20). At room temperature the etch rate of the titanium from the CrC sputter System is approximately 8500Å/min. Therefore an etch time of 20 seconds was required to etch through the titanium. A 20% overetch (additional 4 seconds, for a total etch time of 24 seconds) was included to ensure that no titanium residue remained (any remaining residue could short the top and bottom electrodes). Lastly, the photoresist was removed using the standard photoresist removal process. An optical image of the resulting bottom electrode structure is shown in Fig. 5.1.

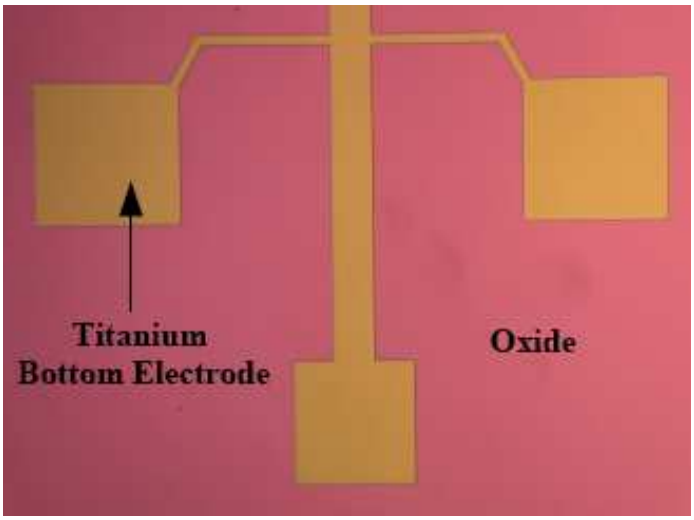

Figure 5.1. Optical image of titanium (2500Å) bottom electrode on oxide (5000Å)

Polymer Dielectric Module

The polymer dielectric module involved dissolving the PEVA into a liquid, spining the PEVA on the wafer, depositing and pattering an etch mask, and plasma etching the polymer. Each of these steps is described below.

- **PEVA Dissolve**. The PEVA came from the manufacturer in solid pellets. To get the PEVA into liquid form, 5 grams of pellets were dissolved in 80mL of toluene by heating to 50°C and stirring (note: heating is toluene is very dangerous because toluene is explosive – and toluene is a carcinogen, so this needs to be done in a ventilated area). The ratio of PEVA and toluene was chosen because it yielded a 1μm-thick film when spun on a wafer.
- **PEVA Application**. The PEVA was spun on the wafer (covering the bottom electrode) using the spin coater in the cleanroom (3500RPM for 30 seconds). A solvent bake-out of 75°C for 2 minutes was then done on a hotplate. This resulted in a uniform film that was 1μm thick. Step coverage of the PEVA over the bottom electrode was sufficient because the PEVA was four times thicker than the bottom electrode. The PEVA was baked for 5 minutes at 75°C on a hotplate to bake out some of the solvents.
- **Etch Mask Deposition & PEVA Patterning**. Because photoresist could not be directly patterned on the PEVA (to serve as an etch mask), an aluminum etch mask had to be used. 500Å of aluminum was deposited on the PEVA using the CrC Sputter System (8 minute deposition at 50W DC and 5mTorr process

pressure). Resist was patterned on the aluminum using the standard 1μm photolithography process and the polymer photomask. A hard bake at 75°C for 4 minutes used. A lower temperature of 75°C was used from this point on because the glass transition temperature of PEVA is 85°C, and exceeding this would cause the PEVA to liquefy and possibly flow. The aluminum was etched using the standard aluminum etch. The etch time was approximately 6 seconds (including a 20% over-etch). Photoresist was removed from the aluminum using the standard photoresist removal process. Note, this resist removal with solvents did not remove the PEVA. The PEVA was etched in the Branson barrel etcher. The parameters used were an RF forward power of 50W and a process pressure of 500mTorr. The etching chemistry was 80sccm of CF_4 and 20sccm of O_2. Typically only O_2 is used to etch organic polymers; however, the addition of CF_4 greatly increases the etch rate. The wafer was placed horizontally in the chamber on a beaker (which raised it up so that it sat in the center of the chamber). The etch time for 1μm of PEVA at these conditions was 4 minutes and 30 seconds (for edges) and 5 minutes for the center of the wafer. A total etch time of 6 minutes was used to ensure that all of the PEVA was removed. An optical image of the sensor at this point is shown in Fig. 5.2, which demonstrates that the aluminum etch masks are still intact.

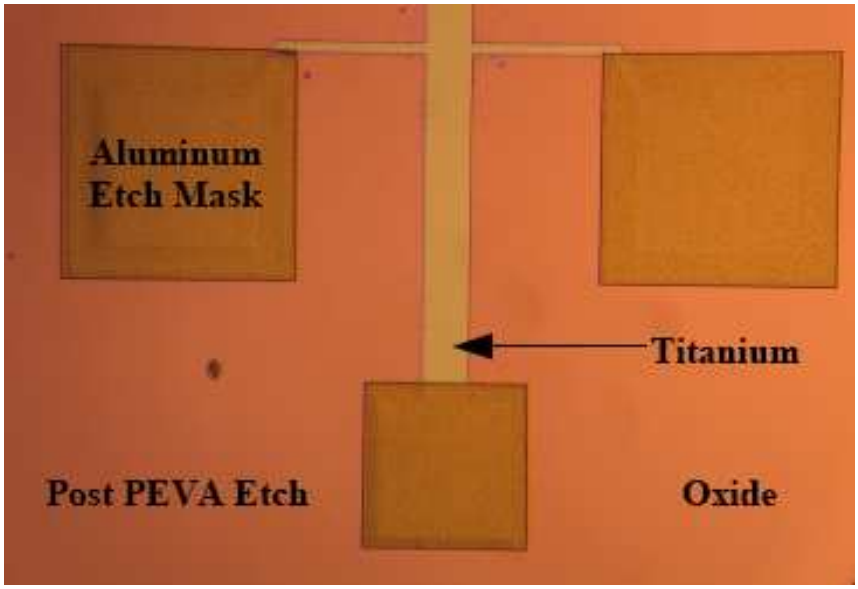

Figure 5.2. Optical image of aluminum etch masks (500Å) after PEVA etch

After a visual inspection to confirm that no PEVA residue was present on the wafer after etching, the aluminum etch mask was removed using the standard aluminum etch. Lastly, the PEVA was hard baked for 30 minutes at 75°C to harden the polymer. This was necessary so that it was more resistant to the aluminum etch for the top electrode. An optical image of the sensor after the Polymer Dielectric Module fabrication is shown in Fig. 5.3.

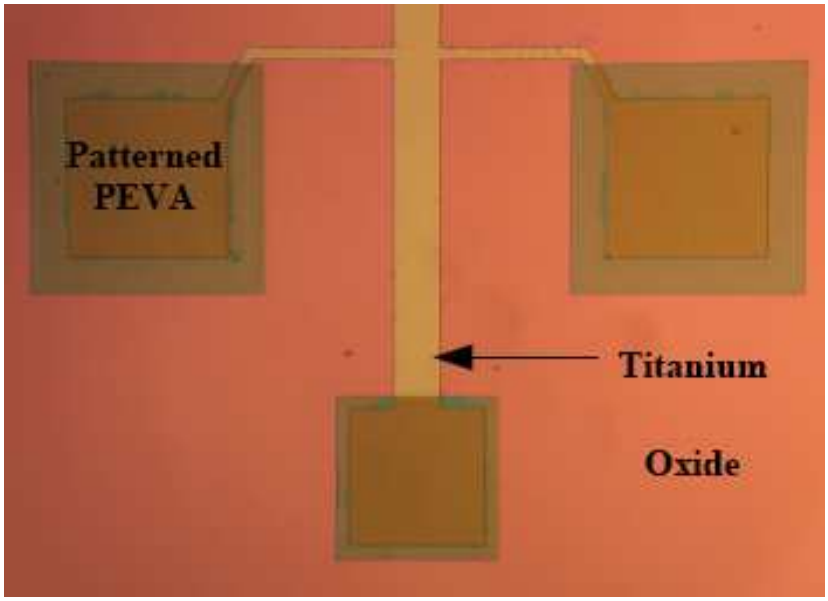

Figure 5.3. Optical image of sensor after PEVA (1μm-thick) patterning

Top Electrode Module

The Top Electrode Module involves depositing and pattering aluminum, as described below.

- **Aluminum Deposition and Patterning**. 2500Å of aluminum was deposited on the wafer using the CrC Sputter System (approximately 35-minute deposition at DC power of 50W and process pressure of 5mTorr). The aluminum is patterned using the standard 1μm photolithography process with the top electrode photomask. The pre-exposure soft-bake was 75°C for 2 minutes. The resist was hard-baked (post-develop) at 75°C for 4 minutes. The standard aluminum etch was used to pattern the aluminum and the wet etch time was 45 seconds. Lastly

the remaining photoresist was removed using the standard photoresist removal process. An optical image of the complete sensor is shown in Fig. 5.4.

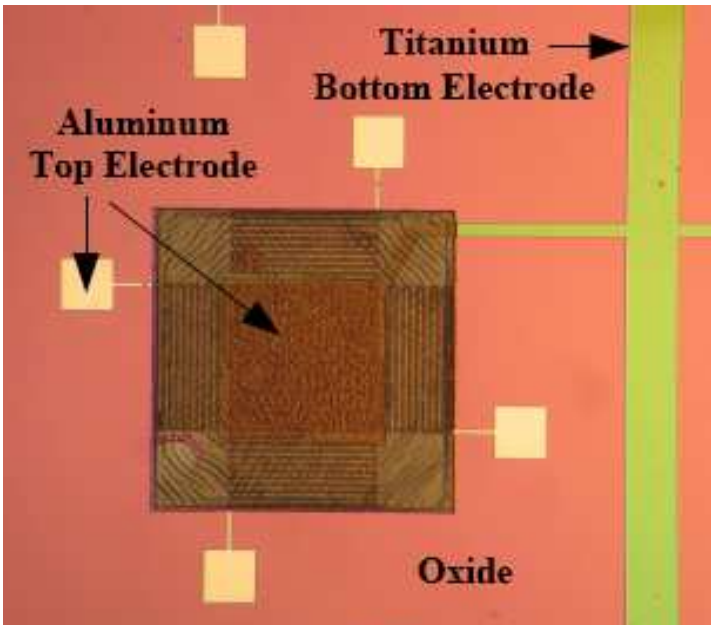

Figure 5.4. Optical image of complete sensor

Figure 5.5 is a SEM image showing the transition of the top electrode aluminum from the PEVA to the field oxide. It is critical that the metal be continuous when transitioning from these two materials so that the sensor can be electrically contacted from the field oxide during testing.

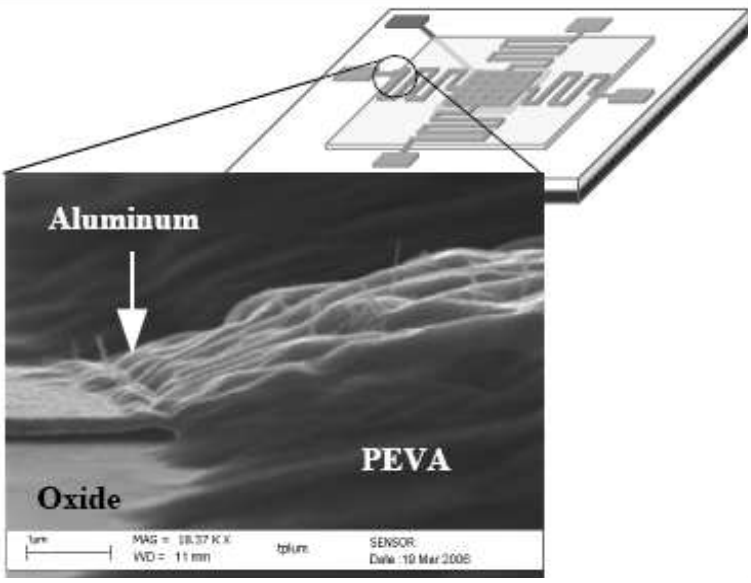

Figure 5.5. SEM image of continuous top electrode transition from PEVA to oxide

Figure 5.6 is a SEM image of the springs and analyte access holes.

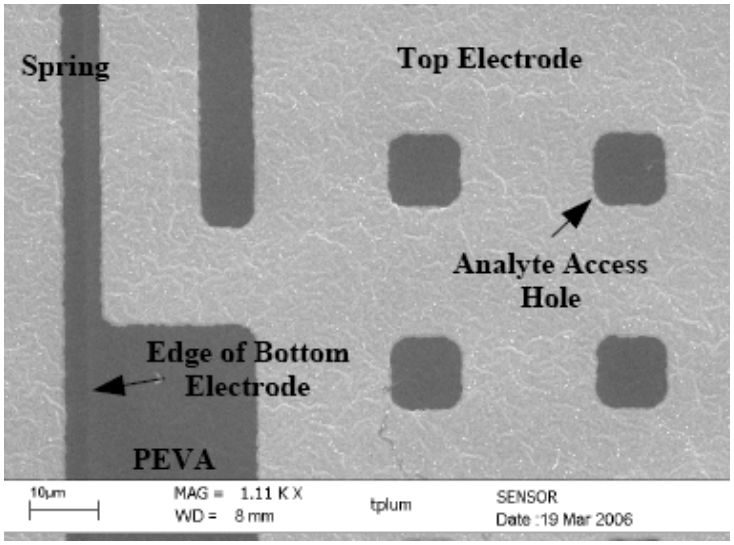

Figure 5.6. SEM image of spring and analyte access holes

Review of Iterations Prior to Final Sensor Integration

All data, including the process integration section in Chapter 3, the sensor fabrication modeling in Chapter 4, and the fabrication presented up to this point in this chapter pertains to the final process integration scheme that was used. However, three significant iterations occurred prior to the settling on a final process flow. This section briefly describes these iterations to demonstrate some of the problems encountered in during the fabrication and to present the engineering solutions to fix the problems.

Iteration 1: Thick PEVA, Poor Step Coverage

The first iteration of the sensor yielded a problem at the top electrode metal deposition. It was noted that (1) the PEVA was twice as thick as measured with the NanoSpec, (2) the etch profile of the PEVA was more vertical than expected, and (3) that the aluminum (5000Å) was not continuous. The PEVA thickness was easy to address by simply diluting the existing PEVA down with toluene. The unexpected etch profile was traced back the aluminum wet etch used to remove the etch mask. For some reason, this caused the somewhat rounded profile to become abruptly vertical. Therefore, this presented a step coverage issue so severe that the metal was discontinuous as it stepped down from the PEVA to the oxide, as seen in Fig. 5.7.

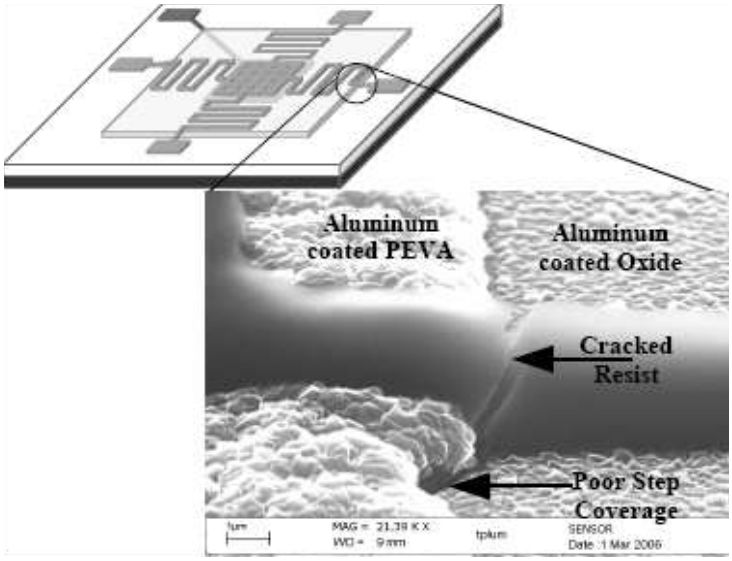

Figure 5.7. Poor step coverage and cracked resist at the PEVA/Oxide interface

Iteration 2: Thinner PEVA, PEVA Etch Mask Left In Tact

To address the problems of Iteration 1, more process development with the PEVA was done until a 1μm thickness was achieved. Secondly, a thicker (10000Å) aluminum would be used to attempt to achieve continuity from the PEVA to the oxide. Lastly, since the removal of the etch mask (for pattering PEVA) caused a dramatic change in the etch profile of the PEVA, it was attempted to leave the mask in place (since it was only 500Å and 10000Å of aluminum would be directly deposited on top of it). The resulting profile of the *pre-metal-etched* top electrode (10000Å of aluminum on PEVA) is shown in Fig. 5.8.

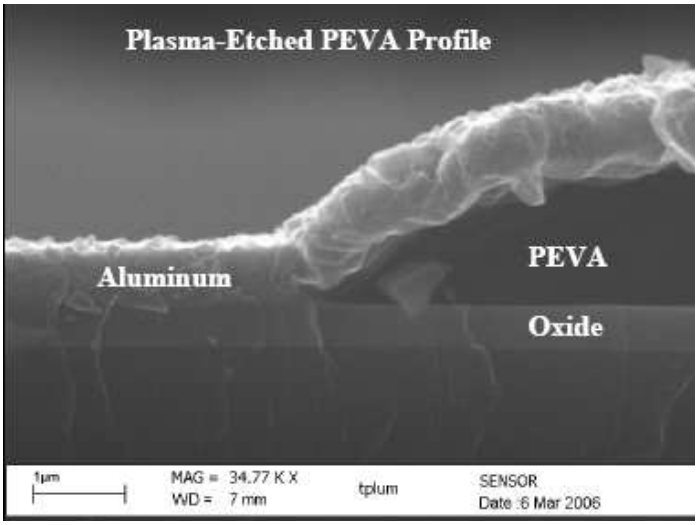

Figure 5.8. Top electrode metal continuity at PEVA edge prior to electrode etch

Figure 5.8 suggests that leaving the etch mask in place may have solved the problem of the abrupt sidewall profile of the PEVA shown in Fig. 5.7. However, directly after the aluminum (top electrode) etch, it was observed that again that the aluminum was discontinuous at the PEVA/oxide interface, as shown in Fig. 5.9.

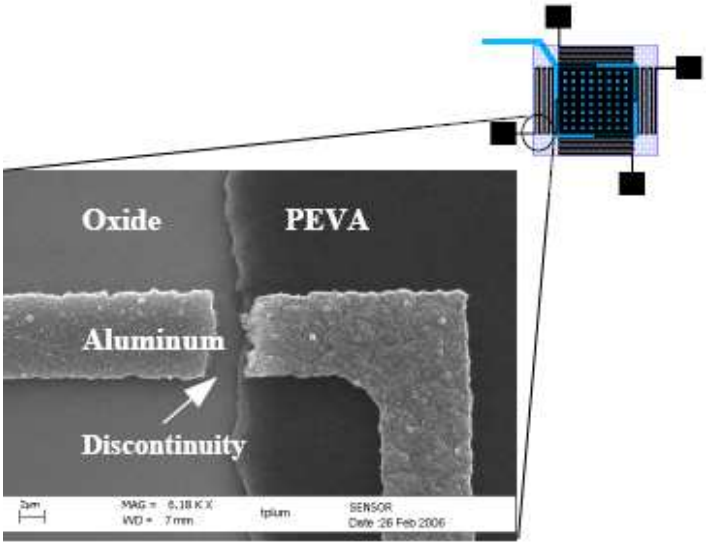

Figure 5.9. Discontinuity at PEVA/Oxide interface

It was then observed that after the top electrode etch, the PEVA had laterally shrunk by several microns, even though it remained well intact in the horizontal direction. From this it is hypothesized that once the top electrode etched entirely through, the etchant caused the PEVA to quickly shrink/shrivel/or etch laterally by several microns. This allowed the aluminum etchant underside access to the metal, which it then etched entirely through. This suggested that there was a problem with using PEVA as an etch stop for the top electrode etch. To address these problems, Iteration 3 was used.

Iteration 3: Resist Buffer Layer

Since contact with the aluminum etchant caused a significant lateral reduction in the size of the PEVA, it was surmised that a buffer film could be placed between the PEVA and the top electrode metal (using the same PEVA photolithography mask). That

way, the PEVA would never see the final aluminum etch. To expose the PEVA to the atmosphere, a plasma etch of the buffer film would be used. To test this process, photoresist was used as a buffer. The addition of the buffer layer did prevent the etching/breaking of the metal as it went from the PEVA to the oxide. However, interaction between the PEVA and resist (during bakes) caused a lot of bubbles due to out-gassing of the polymers. This yielded very unattractive and non-uniform devices. In effort to address this, a longer baking time (from 5 minutes to 30 minutes at 75°C) of the PEVA was tried prior to applying the resist buffer layer. It was noted that this longer bake made the PEVA more resilient to the aluminum etch during the aluminum mask removal (post PEVA etch). This suggested that perhaps the PEVA was capable of withstanding the aluminum etch if it was baked for a considerably longer time. This lead to the fourth and final iteration.

Iteration 4: Removal of Resist Buffer Layer, Final Integration Scheme

Iteration 4 was the final sensor integration scheme. The resist buffer layer was removed and a 30-minute hard bake at 75°C (after the PEVA was etched) was implemented. This made the PEVA resistant enough to the aluminum etching of the top electrode. The details of this iteration are the ones that have been described in Chapter 3, 4 and 5. Figure 5.10 demonstrates (compared with Fig. 5.9) that the aluminum of the top electrode is continuous at the PEVA/Oxide interface.

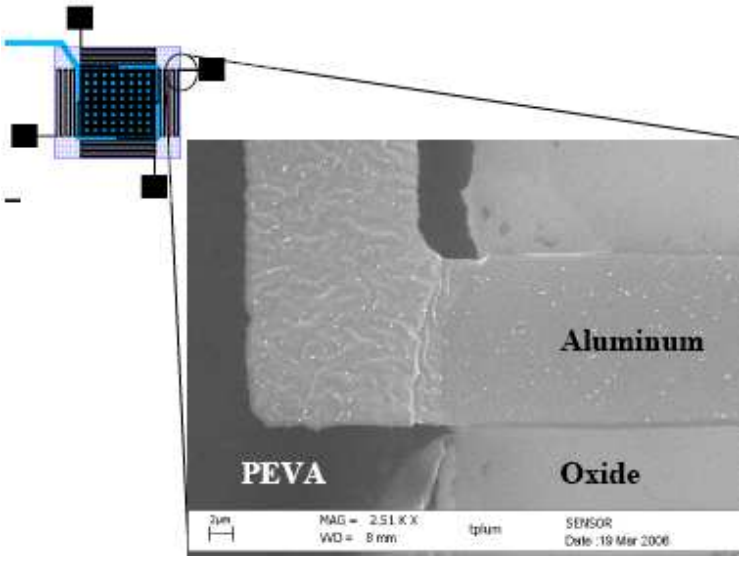

Figure 5.10. Aluminum continuity at PEVA/Oxide interface

Summary

Chapter 5 has provided a detailed description of the fabrication process used to create a functional sensor. Many images have been used to illustrate the fabrication as well. Lastly, a review of the iterations required to reach a successful design was presented in effort to show the difficulty of developing a process like this.

CHAPTER 6: SENSOR TESTING

The objective of testing was to prove that the sensor responded as expected. Expectations were that:

- The capacitance would decrease when exposed to low permittivity analytes that have been shown to cause PEVA to swell.
- The capacitance would not change when exposed to analytes that are not readily absorbed by PEVA.

Test Set-Up

Electrical contact to the sensors was achieved by probing them on the wafer. One probe was placed on the bottom electrode pad and one probe on a top electrode pad. The probes were connected to an HP 4284A LCR meter. All testing was done with 1V (AC) at a frequency of 1kHz. The noise floor of this meter was approximately 5fF (or less) during testing. Because of the potential hazards associated with the analytes (octane and acetone), the probe station was placed in a vented environment (the spin-coater enclosure in the cleanroom).

To deliver the analytes, it would be desirable to build a vapor delivery system, as shown in Fig. 6.1.

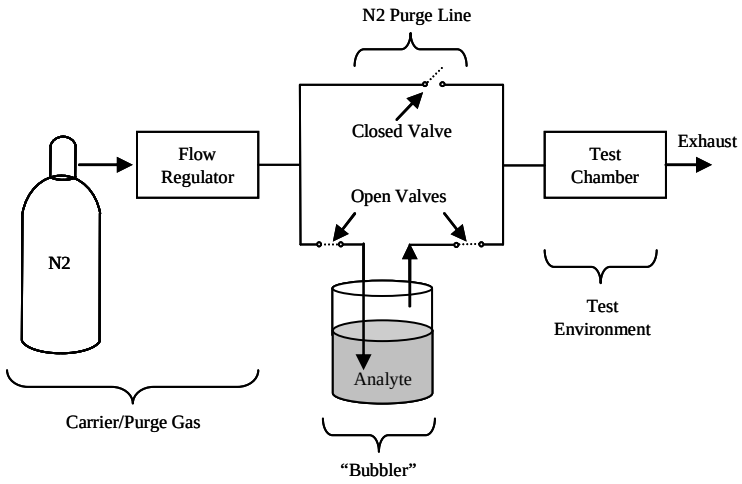

Figure 6.1. Diagram of an ideal analyte delivery system

However, due to the complexity and cost of this (noting that all gas lines must be stainless steel because the analytes attack plastics), a system like this was not built for this preliminary testing. Instead, a crude, proof-of-concept test was performed, which involved dropping a small drop of liquid solvent on the sensor and recording the capacitance from the LCR meter every minute until the capacitance reached equilibrium. Unfortunately, precise volumes of analytes could not be delivered to the sensor each time, so gathering quantitative data was not possible. However, qualitative data could be gathered. This method of testing could be described as an impulse test – quickly exposing the sensor to a large concentration of the analyte and measuring the response over a period of time.

Two different types of sensing structures were tested. The first type of sensors had 2μm of PEVA as the capacitors' dielectrics. The other type of sensors had a 1μm

PEVA layers. The sensors were exposed to octane and acetone, which are classified as volatile organic compounds. These analytes were chosen due to the relationship of their permittivities relative to PEVA. PEVA has a permittivity of approximately 2, as found in literature and verified with the Ellipsometer in the cleanroom. Octane has permittivity of approximately 1.1, which is less than PEVA. Acetone has a permittivity of approximately 20, much larger than PEVA. Octane has been shown to cause PEVA to swell [8]. Since its permittivity is less than PEVA, it was expected that swelling would dominate the capacitive change, even though the net permittivity of the polymer would increase (because of the addition of the absorbed octane). No data was found in literature on PEVA's response to acetone; however, during the fabrication it was noted that acetone did not dissolve PEVA (implying that it does not absorb into PEVA very much and would not cause swelling). Therefore it was expected that acetone would cause minimal changes to the sensors' capacitances.

Testing Results

Sensors with 2μm-thick PEVA layers were tested first. For one of the sensors, the baseline capacitance was 7.40pF (+/- a few femtofarads). The meter read this capacitance for 15 minutes prior to exposure to ensure that the capacitance did not drift. An important distinction with this sensor is that it was "unconditioned" at room temperature – that is, it was not exposed to any analytes after fabrication and prior to testing. The significance of this is that during fabrication, the heat steps bake-out more

liquid in the PEVA than is present at room temperature. Therefore the baseline capacitance would change after testing. The sensor was first tested with acetone and then with octane. The response to the two different analytes is plotted in Fig. 6.2.

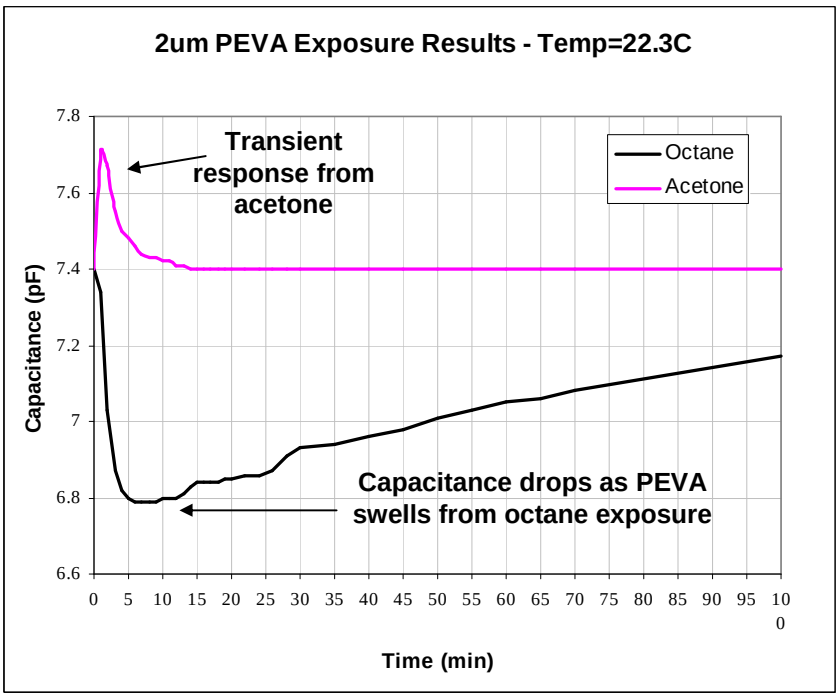

Figure 6.2. 2μm PEVA response to octane and acetone

The data in Fig. 6.2 verifies that the sensor worked as expected, that is the capacitance decreased when exposed to octane (and did not decrease when exposed to acetone). With acetone, there was a spiked increase in capacitance, but the capacitance returned to approximately 7.40pF within 15 minutes. It is believed that the increase in capacitance was due to the liquid acetone filling under-cut voids beneath the top

electrode (near the analyte access holes), which would temporarily increase the capacitance (due to its large permittivity) until the acetone evaporated. Also, note that the capacitance returned to its baseline value, which again supports the thought that very little acetone actually absorbed into the PEVA. Octane, which has a smaller permittivity than PEVA and has been shown to cause PEVA to swell, caused a decrease in capacitance of approximately 600fF, or 8.1% of the baseline capacitance. The de-swelling time was considerably long and relatively linear. Note, that the capacitance never returned to its baseline value because the sensor was unconditioned at room temperature.

The second type of sensor tested used a 1μm-thick PEVA layer. The order of exposure for this sensor was (1) octane exposure on an unconditioned sensor, (2) acetone exposure, and (3) another octane exposure. The response to these exposures is shown in Fig. 6.3.

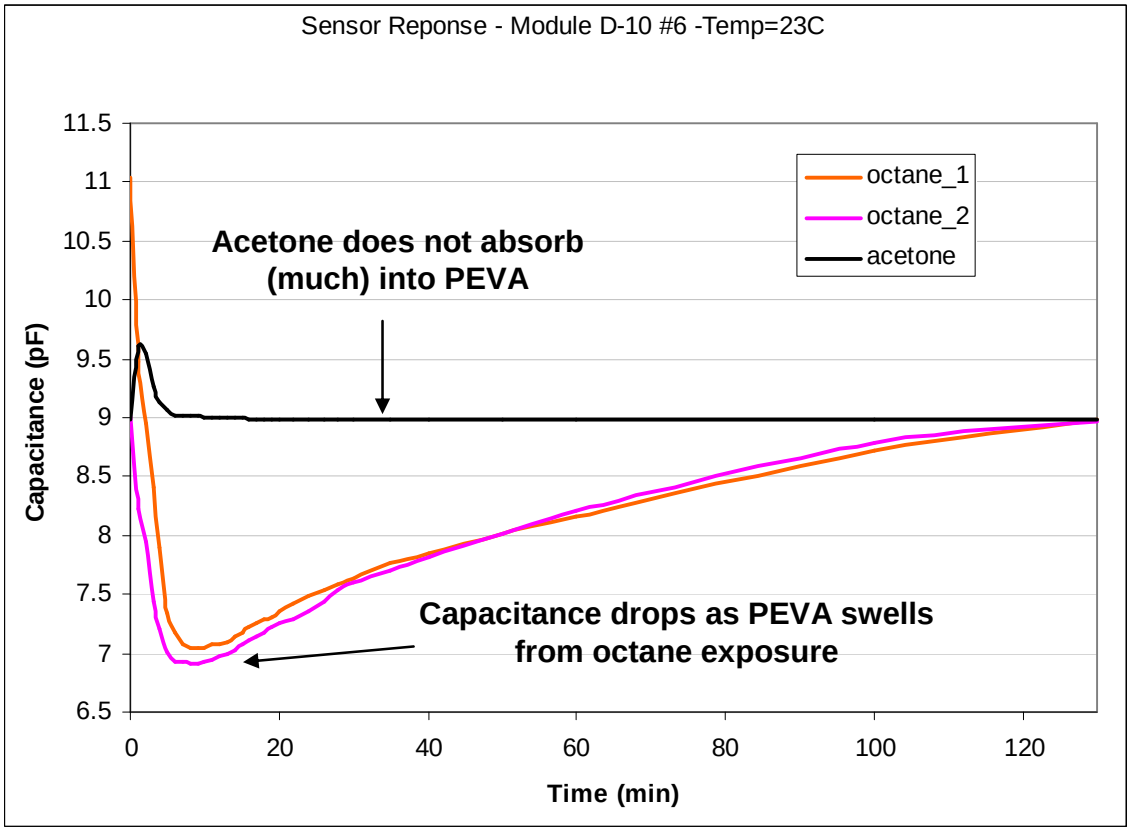

Figure 6.3. 1µm PEVA response to octane and acetone

For the first exposure, the sensor was unconditioned and had a baseline capacitance of 11.04pF. The octane-induced swelling caused a decrease to 7.05pF (a 36% drop). As with the sensor data shown in Fig. 6.2, because the sensor was unconditioned for the first exposure, the capacitance only returned to 9.02pF and not to its baseline of 11.04pF. The sensor was then exposed to acetone and had a response similar to that shown in Fig. 6.2. The pre- and post-acetone exposure capacitance was approximately 9.02pF. Lastly, another octane exposure was performed. This time, the sensor was effectively conditioned from the first octane exposure. The baseline

capacitance was approximately 9.02pF and the octane caused a decrease in capacitance to 6.91pF (a 23%) drop. However, this time, the capacitance did return to its baseline value, demonstrating that conditioning the sensors is important.

Summary

This chapter described the proof-of-concept test set-up and results for the sensor. The sensor responded as expected, decreasing in capacitance when exposed to octane (due to swelling) and staying relatively constant when exposed to acetone (due to lack of absorption of acetone into PEVA). The de-swelling times were considerably long; however, the sensors were exposed to extraordinarily large concentrations of analytes. One possible integration scheme may be to employ polysilicon heaters on the die to assist in desorption time.

CHAPTER 7: SUMMARY AND CONCLUSIONS

Summary

The objectives of the work detailed in this thesis were to research, design, fabricate, and perform proof-of-concept testing of MEMS chemicapacitive sensor to detect volatile organic compounds.

The literature review in Chapter 2 established that polymer-based microsensors are highly sensitive, consume low power, and are somewhat selective. Chemicapacitive sensors to detect changes in permittivity have been reported on. Complex pressure sensors (using capacitance measurements) to detect swelling have been reported; however, the sensor in this work is a considerably easier sensor to fabricate and works is a slightly different way. Lastly a review of polymers as they pertain to chemical sensors was provided.

Chapter 3 detailed the design process, material selection, and process integration. The most important physical aspect of the device design was that of the top electrode, in which the size and density of the analyte access holes and spring dimensions had to be considered. The most important decision pertaining to materials was the selection of PEVA as the dielectric polymer. Lastly, a process flow was proposed that contained

three modules: the Bottom Electrode Module, the Polymer Dielectric Module, and the Top Electrode Module.

Chapter 4 was dedicated to fabrication preparation. The theory and characterization of the required fabrication processes were presented. The processes and sensor fabrication were then modeled with Silvaco Athena.

Chapter 5 detailed the sensor fabrication, including information on the specific tools and parameters that were used. A total of four fabrication iterations were done in an effort to finalize the fabrication process.

Chapter 6 described the proof-of-concept testing that was performed. The sensors responded as expected, decreasing in capacitance due to the swelling of the PEVA film when exposed to octane. Acetone was used to show that the sensor's capacitance did not decrease when exposed to an analyte that does not readily absorb into PEVA. This demonstrates selectivity of the sensor.

Future Work

Future work for sensor design and fabrication could include using different polymers as dielectrics to detect different types of chemicals, integrating several different types of polymers on the same die, and integrating polysilicon heaters on the die to reduce de-swelling time. Also, important future work could include building an environment-controlled chamber to perform significant characterization of the sensor.

Conclusion

The sensor design and fabrication was a success. Proof-of-concept testing showed that the sensor worked as expected. The unique feature of this sensor, compared to other capacitive polymer-based sensors, is that it is selective to low-permittivity analytes, and the fabrication is relatively simple.

Due to the complexity and expense of building a reliable test environment, the minimum sensitivity of the devices is not known from the tests that were performed. Because of the inconsistency of delivering the same amount of analytes to the sensors, a conclusion about the optimal top electrode hole spacing and spring design could not be made, but could be the focus of future work.

REFERENCES

[1] M.C. Glenn and J.A. Schuetz, “An IC Compatible Polymer Humidity Sensor,” Technology Digest, Transducers ‘85, Philidelphia, PA, 1985, pp. 217-220.

[2] D.D. Denton, S.D. Senturia, E.S. Anolick, and D. Scheider, “Fundamental Issues in the Design of Polymeric Capacitive Moisture Sensors,” Technology Digest, Transducers ‘85, Philidelphia, PA, 1985, pp. 202-205.

[3] H. Shibata, M. Ito, M. Asakursa, and K. Watanabe, “A Digital Hygrometer Using a Polyimide Film Relative Humidity Sensor,” IEEE Transactions on Instrumentation and Measurement, vol. 45, no. 2. Ap. 1996, pp. 564-569.

[4] T. Boltshauser, C.A. Leme, and H. Baltes, “High Sensitivity CMOS Humidity Sensors with On-Chip Absolute Capacitance Measurement System,” Sensors and Actuators, B, vol. 15-16, 1993, pp. 75-80.

[5] X. Yan, M. Qin, and Q. Huang, “Capacitive Humidity Sensor in CMOS Technology,” Micromachining and Microfabrication Process Technology and Devices, Proceedings of the SPIE, vol. 4601, 2001, pp. 43-47.

[6] S. Chatzandroulis, E. Tegou, D. Goustouridis, and D. Tsoukalas, “Capacitive-type chemical sensors using thin silicon/polymer bimorph membranes,” Sensors and Actuators, B., vol. 103, 2004, pp. 392-396.

[7] D. Goustouridis, S. Chatzandroulis, P. Normand, and D. Tsoukalas, “A miniature self-aligned pressure sensing element,” Journal of Micromechanics and Microengineering, vol. 6, 1996, pp. 33-35.

[8] S.V. Patel, T.E. Mlsna, B. Fruhberger, E. Klaassen, A. Cemalovic, and D. R. Baselt, “Chemicapacitive microsensors for volatile organic compound detection,” Sensors and Actuators, B. Chemical, vol. 96, no. 3, pp. 541-553, Dec 1, 2003.

[9] D.L. McCorkle, R.J. Warmack, S.V. Patel, T.E. Mlsna, S.R. Hunter, and T.L. Ferrell, “Ethanol vapor detection in aqueous environments using micro-capacitors and dielectric polymers,” Sensors and Actuators, B: Chemical, vol. 107, no. 2, June 2005, pp. 892-903.

[10] T.E. Mlsna, “Chemicapacitive Sensor Development,” Seacoast Science, Inc.: A company Profile, April 2005, pp. 1-10.

[11] C. Hagleitner, “CMOS Single-Chip Gas Detection System Comprising Capacitive, Calorimetric, and Mass-Sensitive Microsensors,” PhD Thesis, Swiss Federal Institute of Technology, Zurich, 2002, pp. 1-168.

[12] A. Kummer, A. Hierlemann, and H. Baltes, “Tuning Sensitivity and Selectivity of Complementary Metal Oxide Semiconductor-Based Capacitive Chemical Microsensors,” Analytical Chemistry, vol. 76, no. 9, May, 2004, pp. 2470-2477.

[13] F.P. Steiner, A. Hierlemann, C. Cornila, G. Noetzel, M. Bachtold, J.G. Korvink, W. Gopel, and H. Baltes, “Polymer Coated Capacitive Microintegrated Gas Sensor,” International Conference on Solid-State Sensors and Actuators, Proceedings, v 2, 1995, p 814-817.

[14] A. Koll, A. Kummer, O. Brand, and H. Baltes, “Discrimination of volatile organic compounds using CMOS capacitive chemical microsensors with thickness adjusted polymer coating,” Proceedings of SPIE - The International Society for Optical Engineering, vol. 3673, pp. 308-317, March, 1999.

[15] C. Hagleitner, A. Hierlemann, and H. Baltes, “Single-Chip CMOS Capacitive Gas Sensor for Detection of Volatile Organic Compounds,” Proceedings of IEEE Sensors, First IEEE International Conference on Sensors - IEEE Sensors 2002, Orlando, FL, United States, Jun 12-14 2002, pp. 1428-1431.

[16] A. Hierlemann, D. Lange, C. Hagleitner, N. Kerness, A. Koll, O. Brand, and H. Baltes, “Application-specific sensor systems based on CMOS chemical microsensor,” Sensors and Actuators, B: Chemical, vol. 70, 2002, pp. 2-11.

[17] C. Cornila, A. Hierlemann, R. Lenggenhager, P. Malcovati, H. Baltes, G. Noetzel, U. Weimar, and W. Gopel, “Capacitive sensors in CMOS technology with polymer coating,” Sensors and Actuators, B, vol. 24-25, 1995, pp. 357-361.

[18] C. K. Ho, M. T. Itamura, M. Kelley, and R. C. Hughes, “Review of Chemical Sensors for In-Situ Monitoring of Volatile Contaminants,” SANDIA Report, #SAND2001-0643, Sandia National Laboratories, Albuquerque, NM, 2001, pp. 1-27.

[19] C.K. Ho, L.K. McGrath, C.E. Davis, M.L. Thomas, J.L. Wright, A.S. Kooser, and R.C. Hughes, “Chemiresistor microsensors for in-situ monitoring of volatile organic compounds: Final LDRD Report,” SANDIA Report, #SAND2003-3410, Sandia National Laboratories, Albuquerque, NM, 2003, pp. 1-137.

[20] F. Zee and J. Judy, "MEMS Chemical Gas Sensor," Proceedings of the 13th Biennial University/Government/Industry Microelectronics Symposium, June 20-23, 1999, pp. 150-152

[21] J.A. Dickson and R.M. Goodman, "Integrated Chemical Sensors Based on Carbon Black and Polymer Films Using a Standard CMOS Process and Post-Processing," IEEE International Symposium on Circuits and Systems, vol. IV, Geneva, Switzerland, 2000, pp. 341-344.

[22] J. Janata, "Electrochemical Microsensors," Invited Paper, Proceedings of the IEEE, vol. 91, no. 6, June 2003, pp. 864-869.

[23] A. Koll, A. Schaufelbuhl, H. Schneeberger, U. Munch, O. Brand, H. Baltes, C. Menolfi, and Q. Huang, "Micromachined CMOS Calorimetric Chemical Sensor with On-Chip Low Noise Amplifier," Proceedings of the IEEE Micro Electro Mechanical Systems (MEMS), 1999, pp. 547-551.

[24] N. Kerness, A. Koll, A. Schaufelbuhl, C. Hagleitner, O. Brand, and H. Baltes, "N-well Based CMOS Calorimetric Chemical Sensors," Proceedings of the IEEE Micro Electro Mechanical Systems (MEMS), 2000, pp. 96-101.

[25] C.K. Ho, E.R. Lindgren, K.S. Rawlinson, L.K. McGrath and J.L. Wright, "Development of a Surface Acoustic Wave Sensor for In-Situ monitoring of Volatile Organic Compounds," Sensors, vol. 3, 2003, pp. 236-247.

[26] M. Hoummady, A. Campitelli, and W. Wlodarski, "Acoustic Wave Sensors: design, sensing mechanisms, and applications," Smart Material Struct., vol. 6, 1997, pp. 647-657.

[27] A. Pohl, "A Review of Wireless SAW Sensors," IEEE Transactions on Ultrasonics, Ferroelectrics, and Frequency Control, vol. 47, no. 2, March 2000, pp. 317-332.

[28] R.A. McGill, R. Chung, D.B. Chrisey, P. Matthews, A. Pique, T. Mlsna, and J.L. Stepnowski, "Performance Optimization of Surface Acoustic Wave Chemical Sensors," IEEE Transactions on Ultrasonics, Ferroelectrics, and Frequency Control, vol. 45, no. 5, Sep. 1998, pp. 1370-1380.

[29] S. Ahmadi, C. Korman, M. Zaghloul, and K. Huang, "CMOS Integrated Gas Sensor Chip Using SAW Technology," Proceedings of the 2003 IEEE International Symposium on Circuits and Systems, Bangkok, Thailand, May 25-28 2003, pp. 848-851.

[30] J.D. Adams, G. Parrott, C. Bauer, T. Sant, L. Manning, M. Jones, and B. Roger, "Nanowatt chemical vapor detection with a self-sensing, piezoelectric microcantilever array," Applied Physics Letters, vol. 83, no. 16, Oct. 2003, pp. 3428-3430.

[31] S.S. Bedair and G.K. Fedder, "CMOS MEMS Oscillator for Gas Chemical Detection," Proceedings of IEEE Sensors 2004, vol. 2, 2004, pp. 955-958.

[32] D. Lange, C. Hagleitner, O. Brand, and H. Baltes, "CMOS Resonant Beam Gas Sensing System with On-Chip Self Excitation," Proceedings of the IEEE Micro Electro Mechanical Systems (MEMS), 2001, pp. 547-552.

[33] C. Hagleitner, D. Lange, N. Kerness, A. Kummer, W.H. Song, A. Hierlemann, O. Brand, and H. Baltes, "CMOS Single-Chip Multisensor Gas Detection System," Proceedings of the IEEE Micro Electro Mechanical Systems (MEMS), 2002, pp. 244-247.

[34] W.D. Callister, Materials Science and Engineering: An Introduction, John Wiley & Sons, 6th edition, July, 1999.

[35] J.W. Grate and M.H. Abraham, "Solubility interactions and the design of chemically selective sorbent coatings for chemical sensors and arrays," Sensors and Actuators: B, vol. 3, 1991, pp. 85-111.

[36] A. Singh and M. Mukherjee, "Swelling Dynamics of Utrathin Polymer Films," Macromolecules, vol. 36, pp. 8728-8731, 2003.

[37] M. Belmares, M. Blanco, W.A. Goddard, III, R.B. Ross, G. Caldwell, S.-H. Chou, J. Pham, P.M. Olofson, and C. Thomas, "Hildebrand and Hansen Solubility Parameters from Molecular Dynamics with Applications to Electronic Nose Polymer Sensors," Journal of Computational Chemistry, vol. 25, no. 15, Nov 30, 2004, pp. 1814-1826.

[38] R.A. McGill, "Choosing polymer coatings for chemical sensors," Chem. Tech., vol. 24, no. 9, pp. 27-37, 1994.

[39] A. Dec and K. Suyama, "A 1.9GHz CMOS VCO with Micromachined Electromechanically Tunable Capacitors," IEEE Journal of Solid-State Circuits, vol. 35, no. 8, Aug. 2000, pp. 1231-1237.

[40] H. Nieminem, V. Ermolov, K. Nybergh, S. Silanto, and T. Ryhanen, "Microelectromechanical capacitors for RF applications," Journal of Micromechanics and Microengineering, vol. 12, 2002, pp. 177-186.

[41] J. Zou, C. Liu, J. Schutt-Aine, J. Chen, and S. Kang, "Development of a Wide Tuning Range MEMS Tunable Capacitor for Wireless Communication Systems," Technical Digest - International Electron Devices Meeting, 2000 IEEE International Electron Devices Meeting, San Francisco, CA, , Dec 10-13 2000, pp. 403-406.

[42] A. Dec and K. Suyama, "Micromachined Electro-Mechanically Tunable Capacitors and Their Applications to RF IC's," IEEE Transactions on Microwave Theory and Techniques, vol. 46, no. 12, Dec. 1998, pp. 2587-2596.

[43] Silvaco International Athena (version 5.6.0.R) and Tonyplot (version 2.10.0.R), copyright 2001.